Cell Reports
Medicine

Article

Management of prostate cancer by targeting 3βHSD1 after enzalutamide and abiraterone treatment

Graphical abstract

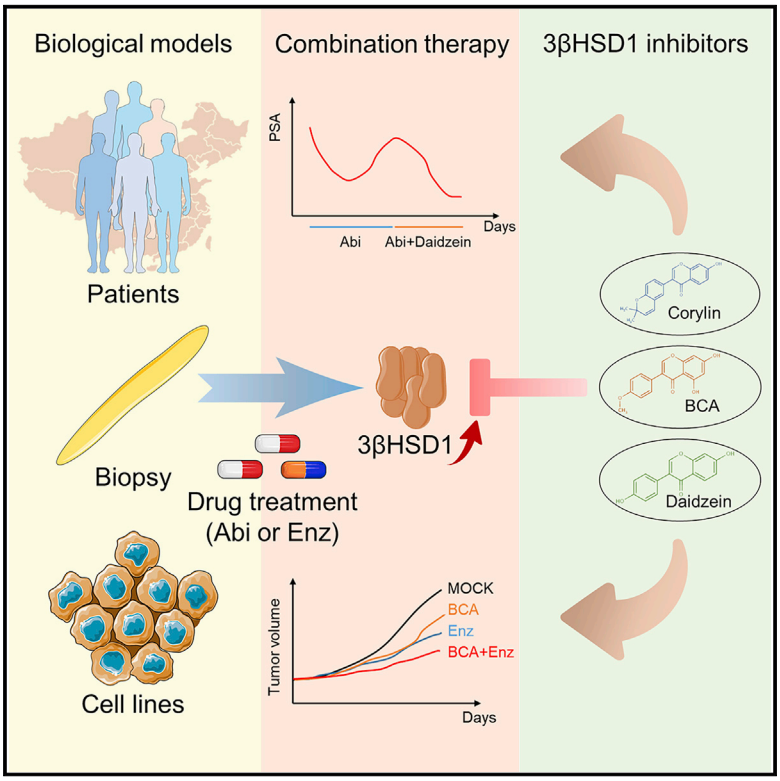

Authors

Zejie Mei, Tao Yang, Ying Liu, ..., Denglong Wu, Shengsong Huang, Zhenfei Li

Correspondence

hssfline@tongji.edu.cn (S.H.), zhenfei.li@sibcb.ac.cn (Z.L.)

In brief

Mei et al. identifies 3βHSD1 as a promising target for prostate cancer treatment even after abiraterone and enzalutamide resistance. The activity of 3βHSD1 increases after long-term treatment of enzalutamide and abiraterone. Biochanin A suppresses 3βHSD1 activity and inhibits prostate cancer progression, shedding light on further disease management and dietary advice.

Highlights

- Increasing 3βHSD1 impairs the efficacy of abiraterone and enzalutamide
- Accelerated abiraterone metabolism promotes drug resistance
- Biochanin A inhibits 3βHSD1 to regulate androgen and abiraterone metabolism
- Biochanin A inhibits PSA increases in abiraterone-resistant patients

Mei et al., 2022, Cell Reports Medicine 3, 100608
May 17, 2022
https://doi.org/10.1016/j.xcrm.2022.100608

CellPress

Cell Reports Medicine

CellPress
OPEN ACCESS

Article

Management of prostate cancer by targeting 3βHSD1 after enzalutamide and abiraterone treatment

Zejie Mei,[1,5] Tao Yang,[2,5] Ying Liu,[2] Yuanyuan Gao,[1] Zemin Hou,[1] Qian Zhuang,[1] Dongyin He,[1] Xuebin Zhang,[1] Qilong Tan,[1] Xuyou Zhu,[3] Yingyi Qin,[4] Xi Chen,[2] Chengdang Xu,[2] Cuidong Bian,[2] Xinan Wang,[2] Chenyang Wang,[2] Denglong Wu,[2] Shengsong Huang,[2,*] and Zhenfei Li[1,2,6,*]

[1]State Key Laboratory of Cell Biology, CAS Center for Excellence in Molecular Cell Science, Shanghai Institute of Biochemistry and Cell Biology, Chinese Academy of Sciences, University of Chinese Academy of Sciences, 320 Yueyang Road, Shanghai 200031, China
[2]Department of Urology, Tongji Hospital, School of Medicine, Tongji University, Shanghai 200065, China
[3]Department of Pathology, Tongji Hospital, School of Medicine, Tongji University, Shanghai 200065, China
[4]Department of Health Statistics, Second Military Medical University, No. 800 Xiangyin Road, Shanghai 200433, China
[5]These authors contributed equally
[6]Lead contact
*Correspondence: hssfline@tongji.edu.cn (S.H.), zhenfei.li@sibcb.ac.cn (Z.L.)
https://doi.org/10.1016/j.xcrm.2022.100608

SUMMARY

Novel strategies for prostate cancer therapy are required to overcome resistance to abiraterone and enzalutamide. Here, we show that increasing 3βHSD1 after abiraterone and enzalutamide treatment is essential for drug resistance, and biochanin A (BCA), as an inhibitor of 3βHSD1, overcomes drug resistance. 3βHSD1 activity increases in cell lines, biopsy samples, and patients after long-term treatment with enzalutamide or abiraterone. Enhanced steroidogenesis, mediated by 3βHSD1, is sufficient to impair enzalutamide function. In patients, accelerated abiraterone metabolism results in a decline of plasma abiraterone as disease progresses. BCA inhibits 3βHSD1 and suppresses prostate cancer development alone or together with abiraterone and enzalutamide. Daidzein, a BCA analog of dietary origin, is associated with higher plasma abiraterone concentrations and prevented prostate-specific antigen (PSA) increases in abiraterone-resistant patients. Overall, our results show that 3βHSD1 is a promising target to overcome drug resistance, and BCA suppresses disease progression as a 3βHSD1 inhibitor even after abiraterone and enzalutamide resistance.

INTRODUCTION

Prostate cancer is the most common cancer among men in the US, and its incidence is rapidly increasing in China.[1,2] Androgen-deprivation therapy (ADT) deprives the prostate of testosterone synthesized by the testis. However, some tumor cells are fueled by dehydroepiandrosterone (DHEA), originating from the adrenal gland, which leads to dihydrotestosterone (DHT) synthesis and the development of castration-resistant prostate cancer (CRPC).[3] Abiraterone and enzalutamide, which suppress steroidogenesis and androgen receptor (AR), respectively, have been approved for the treatment of CRPC.[4,5]

However, despite a tumor response to abiraterone and enzalutamide, drug resistance eventually occurs. Although an increasing incidence of neuroendocrine prostate cancer has been reported, AR-positive adenocarcinoma is still the dominant subtype even after abiraterone or enzalutamide resistance develops.[6–8] The intratumoral androgen concentration is high, and increasing prostate-specific antigens (PSAs) remains an important clinical indicator for disease progression once abiraterone or enzalutamide resistance arises.[9,10] However, previous studies have shown that abiraterone achieved limited clinical efficacy in patients with enzalutamide resistance and vice versa.[11–13] Such findings indicate that the mechanisms underlying resistance may be common to both these next-generation AR pathway inhibitors (ARPIs).[14]

Steroidogenic enzymes are logical potential targets to overcome abiraterone and enzalutamide resistance. The most challenging questions are how to identify an ideal target among the dozens of steroidogenic enzymes and how to prove clinical relevance. Recently, a gain of function of the *HSD3B1* (A1245C) variant was identified as a potential predictive biomarker for treatment response and disease progression.[15,16] The enzyme 3βHSD1 regulates both steroidogenesis and abiraterone metabolism and so may be involved in resistance to abiraterone and enzalutamide.[3] However, the regulation and involvement of 3βHSD1 in patients with either abiraterone or enzalutamide resistance has not been investigated. Thus, whether 3βHSD1 is a useful therapeutic target to overcome abiraterone and enzalutamide resistance remains elusive.

In this study, we investigated drug-resistance mechanisms in prostate cancer cell lines and patients to identify potential targets for prostate cancer treatment. Related inhibitors were identified, and their function in overcoming drug resistance was explored.

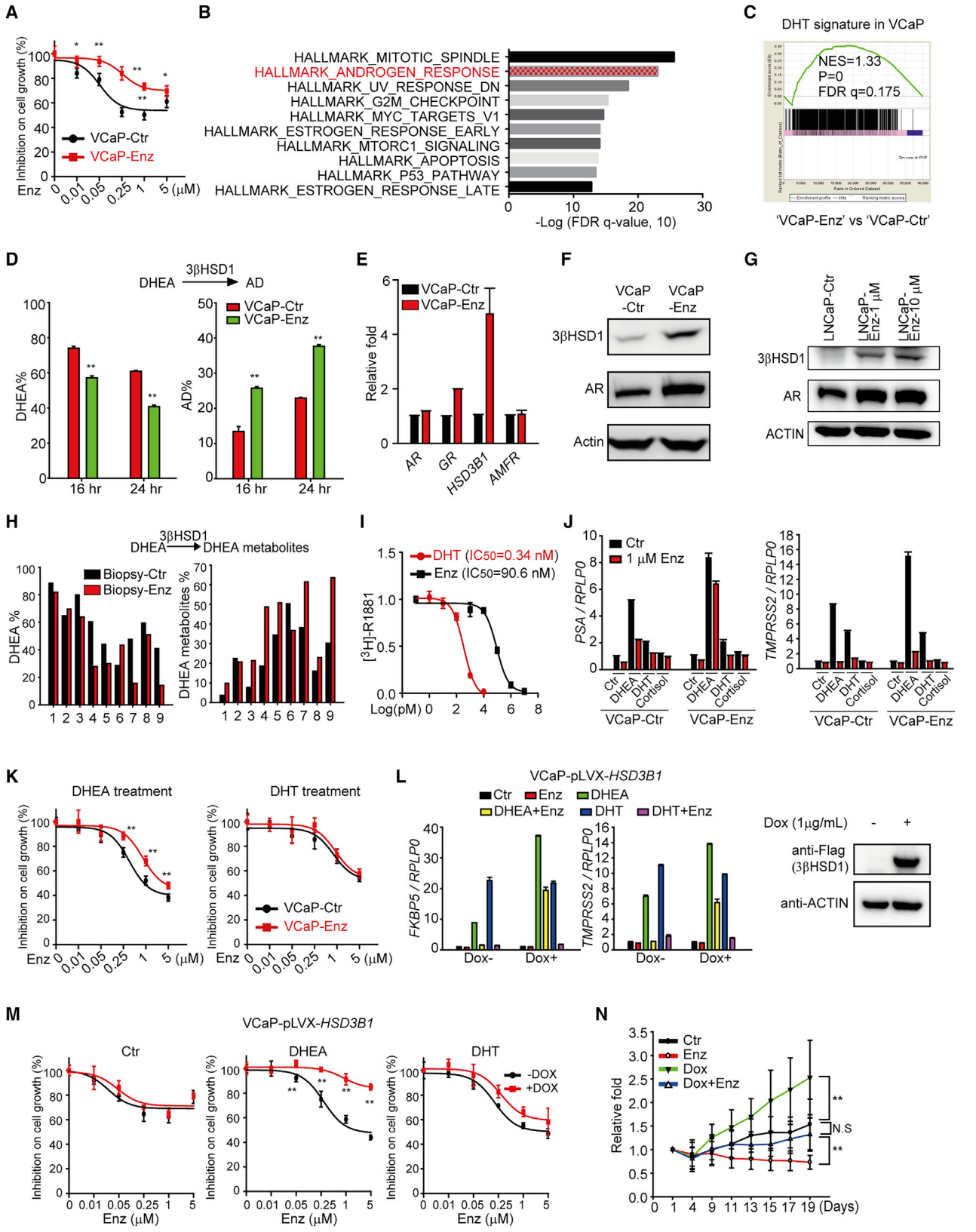

(legend on next page)

RESULTS

Enhanced 3βHSD1 activity after enzalutamide treatment

To investigate mechanisms underlying enzalutamide resistance, vertebral cancer of the prostate (VCaP) cells were treated with 1 μM enzalutamide or ethanol for more than 3 months. The control cells (VCaP-Ctr) were more sensitive to enzalutamide compared with the enzalutamide-resistant cells (VCaP-Enz), as indicated by the cell-growth assay (Figure 1A). The differences in the transcriptome between VCaP-Enz and VCaP-Ctr cells were analyzed with RNA sequencing.[17–21] The AR pathway was enriched in VCaP-Enz cells (Figures 1B and 1C).[22] Steroidogenesis was further investigated to explain the activated AR signaling in VCaP-Enz cells. DHEA was more efficiently converted to androstenedione (AD) in VCaP-Enz cells, indicating increased 3βHSD1 activity in VCaP-Enz cells (Figures 1D and S1A). 3βHSD1 mRNA and protein expression were determined; VCaP-Enz cells expressed more 3βHSD1, consistent with the potent 3βHSD1 activity and the activated AR pathway in VCaP-Enz cells (Figures 1E and 1F). These data together demonstrate that long-term enzalutamide treatment of VCaP cells leads to increased expression of 3βHSD1.

To explain the increased 3βHSD1 abundance and AR signaling in VCaP-Enz cells, the regulation of 3βHSD1 was investigated. Neither the gain of function due to a mutation of *HSD3B1* (A1245C) nor the DNA methylation status of the *HSD3B1* promoter was altered in VCaP-Enz cells (Figures S1B and S1C).[23] An enrichment of AR after androgen stimulation around the *HSD3B1* locus was detected in LNCaP and VCaP cells (GEO: GSE55062, GSE28126, GSE62492, and GSE69043; Figure S2A).[24–27] AR enrichment around *HSD3B1* was also observed in human tumor samples (GEO: GSE56288; Figure S2B).[28] The androgen-regulated expression of *HSD3B1* was further confirmed in different VCaP and LNCaP cells (Figures S2C–S2E). Thus, long-term enzalutamide treatment selected a subpopulation with higher basal AR signaling activity, which stimulated *HSD3B1* expression as a feedforward loop to counter enzalutamide. To determine whether the enzalutamide-induced 3βHSD1 increase was limited to VCaP cells, LNCaP cells and patient biopsy samples were treated with enzalutamide. An increased abundance of 3βHSD1 was detected in LNCaP cells treated with enzalutamide (1 or 10 μM) for more than 4 weeks (Figures 1G and S2F). Accelerated DHEA metabolism was also observed in the enzalutamide-treated LNCaP cells (Figure S2G). Nine prostate biopsy samples were collected from 4 patients. Each biopsy was split equally and cultured *ex vivo* with 10 μM enzalutamide or ethanol for 1 week. Increased 3βHSD1 activity was observed in 7 out of 9 enzalutamide-treated biopsy samples, as indicated by the accelerated conversion of DHEA to AD (Figure 1H).[10] These data together demonstrate that long-term treatment with enzalutamide frequently results in increased 3βHSD1 activity in prostate cancer cells.

3βHSD1 is sufficient to provide enzalutamide resistance

An increasing expression of *HSD3B1* as disease progressed was observed in patients (Figure S2H).[29] To clarify how the enhanced steroidogenesis impaired the function of enzalutamide, a competition assay was performed. DHT, generated from DHEA, showed much higher affinity for wild-type AR than enzalutamide in VCaP cells (Figure 1I).[30] Thus, enhanced steroidogenesis in VCaP-Enz cells provided more intracellular DHT to significantly antagonize enzalutamide function. Consistently, DHEA-induced AR target gene expression was more potent and resistant to enzalutamide treatment in VCaP-Enz cells (Figure 1J). VCaP-Enz cells were more resistant to enzalutamide when treated together with DHEA but responded comparably to VCaP-Ctr cells when treated with DHT, indicating that enzalutamide was not acting off target in VCaP-Enz cells and that mechanisms related to steroidogenesis were involved in enzalutamide resistance (Figure 1K). These data together suggest that enhanced 3βHSD1-mediated steroidogenesis impairs the efficacy of enzalutamide.

To further demonstrate that 3βHSD1 itself was sufficient to provide enzalutamide resistance, a doxycycline (Dox)-induced 3βHSD1-expressing cell line was established in VCaP cells.

Figure 1. Increasing 3βHSD1 activity impairs enzalutamide efficacy

(A) Cell growth of VCaP-Enz and VCaP-Ctr cells when treated with different concentrations of enzalutamide. VCaP cells were treated with 1 μM Enz (VCaP-Enz) or ethanol (VCaP-Ctr) for more than 3 months.

(B) Pathway enrichment in VCaP-Enz cells.

(C) Higher basal AR signaling activity in VCaP-Enz cells. DHT-upregulated genes in VCaP cells were used as AR-signaling signature genes.

(D) Increased DHEA metabolism in VCaP-Enz cells. Cells were treated with [^{3}H]-DHEA.

(E and F) Increased expression of *HSD3B1* mRNA (E) and 3βHSD1 protein (F) in VCaP-Enz cells.

(G) Abundance of 3βHSD1 in enzalutamide-treated LNCaP cells. LNCaP cells were treated with enzalutamide (1 or 10 μM) for more than 4 weeks.

(H) Increased 3βHSD1 activity in biopsy samples (n = 9 patients) treated with 10 μM enzalutamide for 1 week.

(I) DHT had significantly higher affinity for wild-type AR compared with enzalutamide. VCaP cells were treated with [^{3}H]-R1881 and the indicated drugs. Intracellular radioactivity was measured and normalized to protein abundance.

(J) DHEA activated AR signaling more effectively in VCaP-Enz cells. DHEA, 100 nM; DHT, 1 nM; cortisol, 100 nM.

(K) Cell growth of VCaP-Enz and VCaP-Ctr cells when treated with enzalutamide together with DHEA (200 nM) or DHT (1 nM).

(L) Expression of *HSD3B1* induced by doxycycline (Dox; 1 μg/μL) diminished enzalutamide inhibition of AR signaling in VCaP-pLVX-*HSD3B1* stable cells. DHEA, 200 nM; DHT, 1 nM; Enz, 1 μM.

(M) Expression of 3βHSD1 impaired enzalutamide function in suppressing DHEA-induced cell growth. DHEA, 200 nM; DHT, 1 nM.

(N) Overexpression of 3βHSD1 impaired the inhibition of enzalutamide on DHEA-induced xenograft growth. VCaP-pLVX-*HSD3B1* cells were injected in castrated mice with DHEA pellets for xenograft assay. Ctr group, n = 12; Enz group, n = 14; Dox group, n = 13; Dox + Enz group, n = 13. Dox, 2 mg/mL in water; Enz, 10 mg/kg.

*p < 0.05; **p < 0.01. Results are presented as mean ± SD. Experiments were performed at least three times independently.

See also Figures S1–S3.

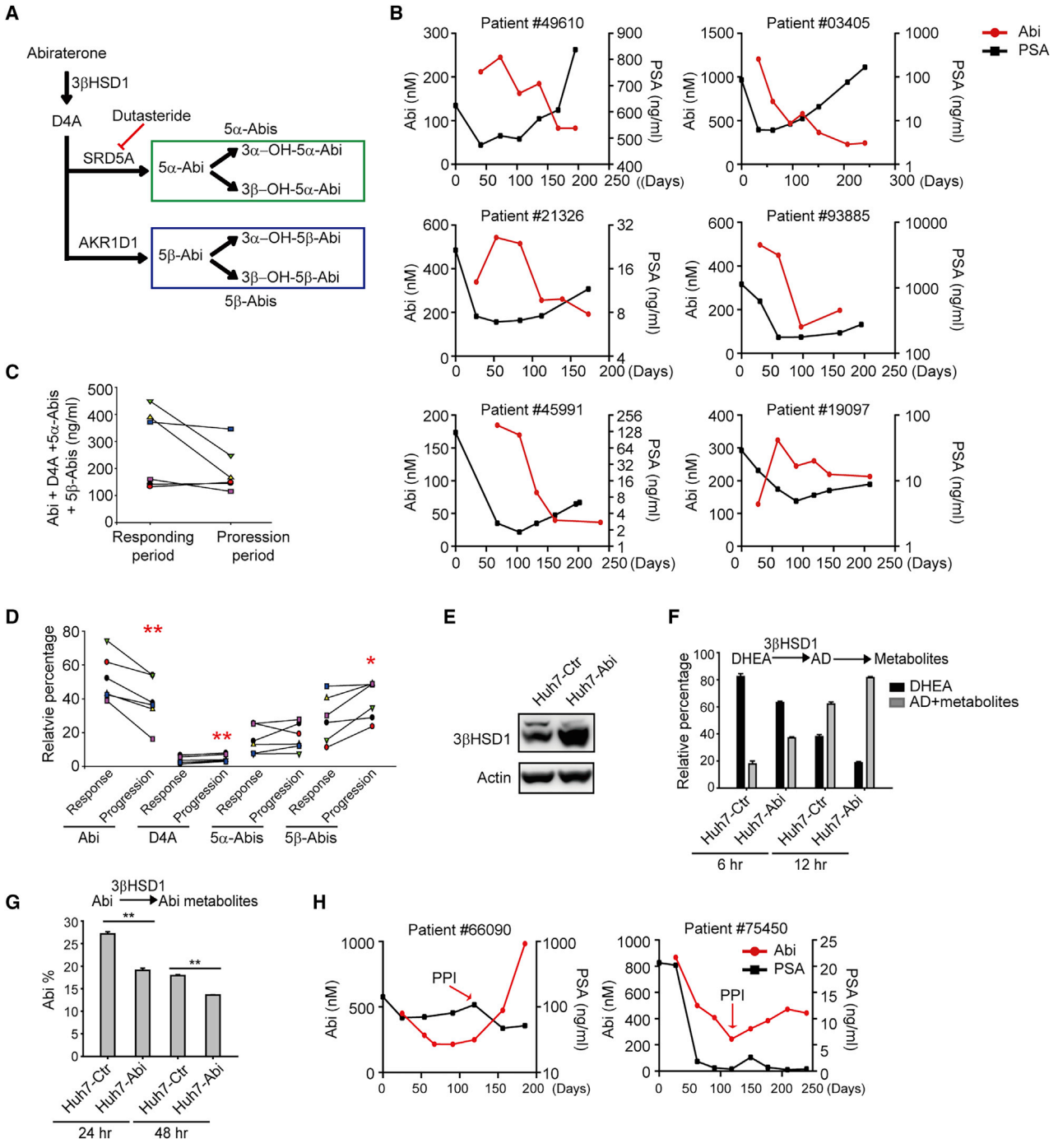

Figure 2. Accelerated abiraterone metabolism facilitates drug clearance in patients

(A) Schema of the steroidal metabolic pathway for abiraterone.

(B) Decline in plasma abiraterone concentration observed in 6 of 11 patients with acquired resistance to abiraterone. Day 0 indicates the baseline PSAs before abiraterone treatment. Plasma samples were collected approximately 3 h after abiraterone administration. Abi, abiraterone.

(C) Plasma concentration of abiraterone and its metabolites before and after abiraterone resistance in the 6 patients. The mean abiraterone metabolite quantity in each patient during the response period (decreasing PSAs) and progression period (increasing PSAs) was calculated and compared.

(D) Relative percentage of abiraterone and its metabolites before and after abiraterone resistance. 5α-Abis, 5α-Abi, and its downstream metabolites; 5β-Abis, 5β-Abi, and its downstream metabolites.

(E) Western-blot analysis of 3βHSD1 expression in abiraterone- or ethanol-treated Huh7 cells. Huh7 cells were treated with 1 μM abiraterone (Huh7-Abi) or ethanol (Huh7-Ctr) for more than 2 weeks before the detection of 3βHSD1.

(legend continued on next page)

The induction of 3βHSD1 expression impaired enzalutamide's ability to antagonize DHEA- but not DHT-induced target gene expression and cell growth, which mimicked the results in VCaP-Enz cells (Figures 1L and 1M). The expression of 3βHSD1 led to faster VCaP xenograft growth *in vivo* (Figure 1N). Although enzalutamide suppressed xenograft growth significantly, the Dox-induced 3βHSD1 expression rescued the growth of xenografts (Figures 1N and S3). Together, these data demonstrate that 3βHSD1-mediated steroidogenesis is sufficient to provide enzalutamide resistance.

Accelerated abiraterone metabolism facilitates drug clearance in patients

Currently there is no ideal model to investigate abiraterone resistance in cell lines or mice.[3] To investigate abiraterone-resistant mechanisms in patients, sequential plasma samples were collected from 11 metastatic CRPC (mCRPC) patients to trace the alteration of abiraterone metabolites as disease progresses (Figure 2A; Table S1). The abiraterone plasma concentration declined in 6 of the 11 patients as PSAs increased (Figures 2B and S4A). However, the total amount of plasma abiraterone and its downstream metabolites was comparable during treatment response (PSAs decreasing) and during progression (PSAs increasing), indicating limited alteration in drug absorption (Figure 2C). The relative percentage of plasma abiraterone declined significantly in every patient as PSAs increased, indicating abiraterone metabolism accelerates in patients as disease progresses (Figure 2D). Notably, the percentage of 5β-Abis (5β-Abi + 3α-OH 5β-Abi + 3β-OH 5β-Abi), but not 5α-Abis (5α-Abi + 3α-OH 5α-Abi + 3β-OH 5α-Abi), increased as disease progressed, suggesting increased activity of 3βHSD1 and AKR1D1 in patients (Figures 2D and 2A).

The *HSD3B1* genotype in these 11 patients was determined, and no *HSD3B1* (1245C) was found after abiraterone treatment, consistent with previous reports showing a rare frequency of *HSD3B1* (1245C) in East Asian patients (~2%) (Figure S4B).[31,32] Mechanisms underlying the accelerated abiraterone metabolism were further investigated. The liver is the main organ for drug metabolism. Huh7, a liver cell line, was treated with abiraterone for more than 2 weeks. Expression of 3βHSD1 increased in the abiraterone-treated Huh7 cells (Figure 2E). Potent 3βHSD1 activity in the abiraterone-treated Huh7 cells was confirmed by enhanced conversion of DHEA to AD (Figure 2F). Thus, abiraterone-treated Huh7 cells converted abiraterone to downstream metabolites more robustly (Figure 2G). These data indicate that long-term treatment with abiraterone enhances 3βHSD1 expression and accelerates abiraterone elimination.

The decline in plasma abiraterone concentration was also observed in two other patients with gastrointestinal irritation after the long-term treatment with abiraterone. Both patients showed a trend of PSA progression (Figure 2H). When a proton pump inhibitor (PPI) was added to suppress the gastrointestinal irritation, plasma abiraterone increased in both patients, accompanied by an improved PSA response (Figure 2H). These data indicate that plasma abiraterone concentration is essential to its clinical efficacy.

Dutasteride inhibition of SRD5A partially regulates abiraterone metabolism

Dutasteride (3.5 mg/day), an SRD5A inhibitor, has been reported to effectively regulate abiraterone metabolism by suppressing the conversion of the abiraterone metabolites Δ4-abiraterone (D4A) to 5α-Abi, providing a potential strategy to increase plasma abiraterone and overcome drug resistance (Figure 2A).[33] A total of 19 patients with abiraterone resistance received combination therapy of abiraterone and dutasteride (0.5 mg/day) (Table S2). The combination therapy was successful in 1 patient, with a maximum PSA reduction greater than 30% and a response lasting more than 12 weeks (Figure 3A). However, overall, the effect of the combination therapy was not robust. A limited reduction in the PSA level was observed in 7 of 19 patients (range: -1.9% to -32%) (Figure 3B).

To elucidate why the combination therapy had limited efficacy, plasma levels of abiraterone and its metabolites were determined. Dutasteride, at a dose of 0.5 mg/day, successfully blocked the generation of 5α-Abi in all patients (Figure 3C). In addition, the levels of 5α-Abis significantly decreased after the addition of dutasteride (Figure 3D). However, the percentage of 5β-Abis increased, which hindered the accumulation of abiraterone and D4A (Figure 3D). These data suggest that dutasteride is sufficient to effectively block the generation of 5α-Abis. However, with more abiraterone converted to 5β-Abis, the clinical efficacy of dutasteride was hampered.

A relatively low level of plasma 5α-Abis was noticed in our patient cohort. More 5β-Abis, rather than 5α-Abis, was generated in our patients when treated with abiraterone alone (Figure 3E). Only 5 of 19 patients generated more 5α-Abis than 5β-Abis (Figure 3F). Comparison with the abiraterone metabolite distribution in patients from western countries confirmed the lower level of 5α-Abis in our patient cohort (Figure 3G).[34] The relatively low levels of 5α-Abis indicate that SRD5A is not an ideal target to regulate abiraterone metabolism in our patients.

The differences between patients with or without PSA reduction after combination therapy were further analyzed. Considering the transient clinical response, abiraterone metabolism at baseline and the first month after combination therapy were investigated. These data were available for 18 of the 19 patients. Dutasteride effectively changed the distribution of abiraterone metabolites in one month in all patients, by significantly decreasing the percentage of 5α-Abis, while increasing that of D4A (Figure 3H). Notably, patients with PSA reduction had a lower level of 5β-Abis, indicating low AKR1D1 activity (Figure 3I). Thus, dutasteride increased the percentage of D4A in patients that had PSA reduction (Figure 3I). Furthermore, a higher

(F and G) DHEA (a mixture of 10 nM DHEA and ~20 nM [^{3}H]-DHEA) and abiraterone (100 nM) metabolism in Huh7-Abi and Huh7-Ctr cells. AD, androstenedione. (H) Plasma abiraterone and PSA alteration in patients receiving abiraterone plus PPI. The red arrows indicate the time point of PPI administration. PPI, proton-pump inhibitor.

Experiments were performed at least three times independently. Student's t test. *$p < 0.05$; **$p < 0.01$.

See also Figure S4 and Table S1.

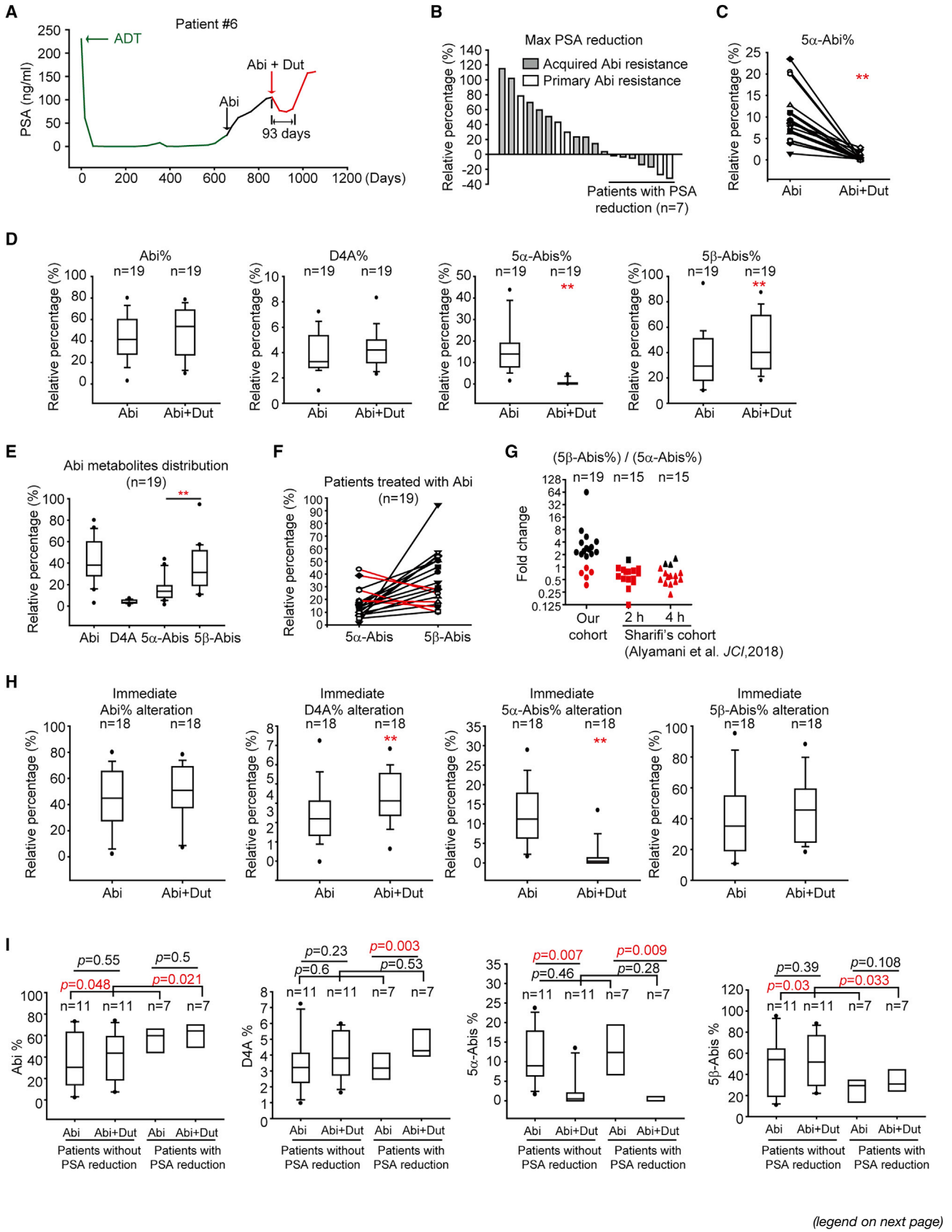

(legend on next page)

percentage of abiraterone was observed in patients with PSA reduction (Figure 3I). These data suggest that the combination therapy would only benefit patients who have a lower level of 5β-Abis.

BCA antagonizes 3βHSD1-related cancer development and enzalutamide resistance

Recently, we revealed that corylin and its derivatives, including biochanin A (BCA) and daidzein, bound to and inhibited 3βHSD1 (Figure 4A).[35,36] BCA, as the most potent 3βHSD1 inhibitor discovered so far, inhibited the conversion of DHEA to AD in a dose-dependent fashion (Figure 4B). Furthermore, BCA suppressed the function of the 3βHSD1 (367T) and 3βHSD1 (367N) isoforms comparably (Figure 4C). An *in vitro* enzyme assay with purified 3βHSD1 protein revealed that BCA competitively inhibited 3βHSD1 (Figure 4D). BCA and corylin showed no direct effect on pregnenolone or AD metabolism, supporting their specific function in steroidogenesis (Figures 4E and 4F). Androgens bind to AR and increase AR abundance.[37] Thus, by suppressing 3βHSD1-mediated DHEA metabolism, BCA antagonized the effect of DHEA on AR abundance in LNCaP and VCaP cells (Figure 4G) and consequently antagonized DHEA's effects on VCaP cell proliferation (Figure 4H). BCA also inhibited DHEA-induced VCaP xenograft growth in mice (Figures 4I and S5A). The function of BCA was also evaluated in C4-2 cells. BCA inhibited DHEA- but not DHT-induced AR target gene expression (Figure S5B). BCA also enhanced the function of enzalutamide to antagonize the DHEA effect (Figure S5C). Furthermore, BCA suppressed DHEA-induced C4-2 xenograft growth (Figure S5D).These data together demonstrate that BCA specifically and potently inhibits 3βHSD1 function to suppress prostate cancer development.

To evaluate BCA antagonism of 3βHSD1-related enzalutamide resistance, BCA and corylin were used to halt 3βHSD1 activity in VCaP-Enz cells. BCA and corylin, together with enzalutamide, inhibited DHEA- but not DHT-induced gene expression more potently in VCaP-Enz cells (Figures 4J and 4K). Furthermore, BCA and corylin suppressed DHEA-induced cell growth together with enzalutamide (Figures 4L and 4M). In mice, BCA and enzalutamide together suppressed VCaP-Enz xenograft growth more than either drug alone (Figures 4N and S5E). Together, these data demonstrate that BCA antagonizes 3βHSD1-related enzalutamide resistance.

BCA regulates abiraterone metabolism to enhance abiraterone efficacy

Investigation of the effect of BCA on abiraterone metabolism showed that BCA inhibited abiraterone metabolism in both LNCaP cells and patient prostate biopsy samples, where D4A was mainly converted to 5α-Abis (Figures 5A and 5B). BCA also inhibited abiraterone metabolism in liver cells, including Huh7 and HepG2, where D4A was mainly converted to 5β-Abis (Figures 5C and 5D). Furthermore, BCA inhibited abiraterone metabolism in mouse and increased the plasma concentration of abiraterone significantly (Figure 5E). For steroidogenesis, BCA and abiraterone synergistically inhibited pregnenolone metabolism in VCaP cells expressing CYP17A. Less DHEA and AD were generated when cells were treated with combination abiraterone and BCA (Figure 5F). Thus, abiraterone and BCA together inhibited pregnenolone but not DHEA-induced target gene expression and cell growth more potently (Figures 5G and 5H). By simultaneously inhibiting drug metabolism and steroidogenesis, BCA enhanced the tumor antagonist effect of abiraterone in mice. Growth of xenografts generated with VCaP cells was more potently suppressed by combination BCA and abiraterone (Figures 5I and S6). These data demonstrate that BCA enhances the efficacy of abiraterone.

Daidzein enhances the clinical efficacy of abiraterone

Daidzein is a BCA analog obtained in the diet, mainly in soybeans and other legumes (Figure 4A). Daidzein inhibited abiraterone metabolism in VCaP and Huh7 cells, although not as potently as corylin and BCA (Figures 6A and 6B). Because daidzein can be acquired in the diet, we measured the plasma concentration of daidzein in 32 patients after abiraterone treatment for ~12 weeks (Table S3). Although daidzein was not detected in the plasma of 20 patients (group I), it was found in the plasma of the remaining 12 patients (group II). Interestingly, in patients

Figure 3. Inhibition of dutasteride on SRD5A partially regulates abiraterone metabolism

(A) Treatments and changes in PSAs in patient 6. Green, androgen deprivation therapy (ADT); black, abiraterone (Abi) treatment; red, abiraterone and dutasteride (Dut) treatment.

(B) Maximum PSA reduction during the combination therapy in 19 patients.

(C) Change in 5α-Abi% after combination treatment. The mean percentage of 5α-Abi in each of the 19 patients during abiraterone treatment or the combination treatment was compared.

(D) The effect of dutasteride on abiraterone metabolism. Average percentages of plasma abiraterone and its metabolites during different treatment periods were compared.

(E) Distribution of abiraterone metabolites in 19 patients at baseline. Plasma samples collected at baseline (patients treated with abiraterone alone before the combination therapy) were used for analysis of abiraterone metabolites. Plasma samples were collected ~3 h after drug administration.

(F) Comparison of the percentages of 5α-Abis and 5β-Abis in each patient receiving abiraterone treatment. The percentages of 5α-Abis and 5β-Abis from the same patients were linked with lines for comparison. Patients with more 5α-Abis than 5β-Abis were marked with red lines.

(G) The ratio of 5β-Abis to 5α-Abis in two patient cohorts. Red, patients with more 5α-Abis than 5β-Abis.

(H) Immediate effect of the combination therapy on abiraterone metabolism. Plasma samples collected at the baseline (Abi) and 1 month after the addition of dutasteride (Abi + Dut) in 18 of the 19 patients were analyzed to evaluate the immediate function of dutasteride.

(I) Distributions of abiraterone and its metabolites in patients with or without PSA reduction after combination therapy. The immediate effect of dutasteride on abiraterone metabolism was compared between patients with and without PSA reduction. The box indicates the median and interquartile range. Whiskers indicate the 5th and 95th percentiles. The percentage of each metabolite was calculated as follows: metabolite/(abiraterone + abiraterone metabolites) × 100%. Student's t test; **$p < 0.01$.

See also Table S2.

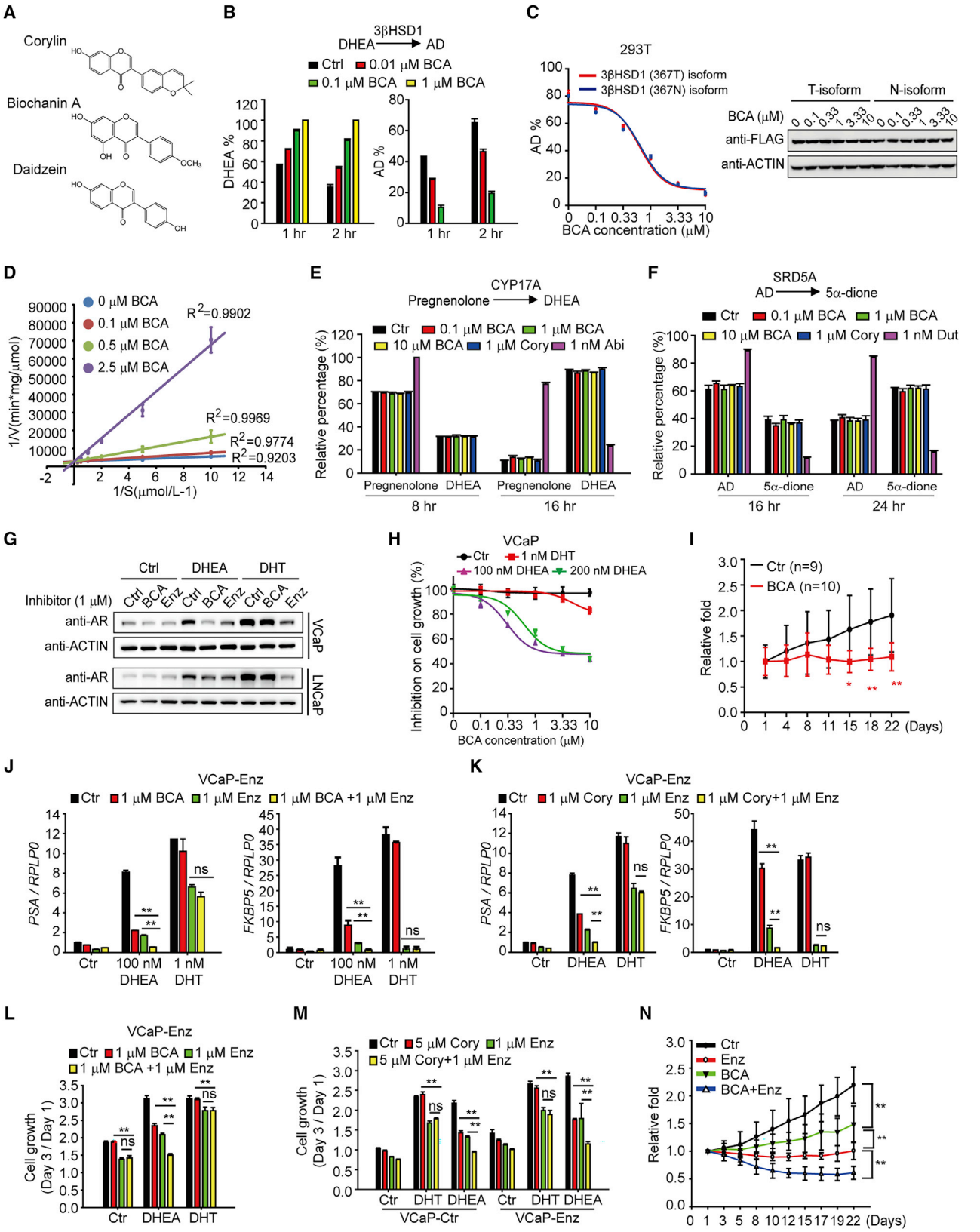

(legend on next page)

in whom daidzein was detected, a higher concentration or relative percentage of abiraterone was also found (Figure 6C). Patients in whom daidzein was detected also tended to have a better response to abiraterone, as indicated by the progression-free survival (Figure 6D). Overall, these data highlight the potential of BCA and its derivatives for regulating abiraterone metabolism and efficacy in patients.

Daidzein is used in clinics in China as an adjuvant therapy for hypertension or osteoporosis. A clinical trial is being conducted to treat abiraterone-resistant patients with daidzein together with abiraterone (ChiCTR: ChiCTR2000034019). Currently, 9 patients have been recruited with a treatment duration of more than 3 months. Daidzein halted PSA increase (n = 1 patient) or reduced PSAs (n = 4 patients) (Figure 6E; Table S4). The dynamic alterations of PSAs after daidzein treatment in 2 patients are shown in Figure 6F. Considering that daidzein more weakly suppresses 3βHSD1 activity, BCA may produce a better clinical response by regulating drug metabolism and steroidogenesis simultaneously.

DISCUSSION

Novel targets and drugs are required to overcome abiraterone and enzalutamide resistance in advanced prostate cancer. Here, we showed that the steroidogenic enzyme 3βHSD1 is essential for drug resistance and that it might be a promising target for prostate cancer management. BCA and its derivatives inhibit 3βHSD1 to suppress prostate cancer development.

The androgen-AR axis remains a significant driver of tumor progression even after abiraterone and enzalutamide resistance develops. However, multiple enzymes are involved in DHT synthesis, and certainly not all of them will be suitable therapeutic targets: dutasteride, an SRD5A inhibitor, was ineffective for prostate cancer.[38,39] Steroidogenic enzyme function has mainly been investigated in prostate cancer cell lines, making it difficult to evaluate clinical relevance. An adrenal-permissive *HSD3B1* (1245C) allele of 3βHSD1 increases protein stability,[23] and the *HSD3B1* genotype in patients receiving ADT is now well established as a predictive biomarker.[16,40–42] However, its correlation with abiraterone response remains controversial.[15,16,43] Furthermore, it is still unclear whether 3βHSD1 is regulated by abiraterone and enzalutamide and whether it may serve as a therapeutic target to overcome abiraterone and enzalutamide resistance. Here, we report that 3βHSD1 expression increases after abiraterone and enzalutamide treatment in preclinical models and patients, highlighting its clinical relevance in disease treatment.

A 3βHSD1-initiated abiraterone metabolic pathway in patients has been found, but its clinical significance is yet to be determined.[33,44] Here, we demonstrated that the increased 3βHSD1 protein expression in abiraterone-treated patients resulted in accelerated abiraterone metabolism and decreased plasma abiraterone concentration, which eroded the efficacy of abiraterone. Clinical approaches to increase plasma abiraterone concentration, such as proton-pump inhibitors (PPIs) and a high-fat diet, have been reported to enhance its clinical efficacy.[45,46] Consistently, previous reports found that patients with abiraterone C_{min} >8.4 ng/mL had a better prognosis than patients with a low C_{min}, indicating that the plasma abiraterone concentration is important to its efficacy.[47,48] However, increasing the dose of abiraterone after drug resistance resulted in no obvious change in the plasma concentration or efficacy.[46,49] This may be due to limitations in drug absorption and accelerated drug metabolism. Thus, regulation of abiraterone metabolism may be a more promising strategy to overcome abiraterone resistance.

Multiple enzymes participate in abiraterone metabolism, and we previously hypothesized SRD5A to be a potential target for regulating abiraterone metabolism to overcome drug resistance.[33] However, we found here that combination therapy with dutasteride and abiraterone benefited only patients with high SRD5A/low AKR1D1 activity. Of note, genomic and metabolic differences were present between patients of different ethnicities. Abiraterone was converted more often to 5β-Abis in East Asian (Chinese) patients, whereas in patients from western countries, more 5α-Abis were generated. Thus, 3βHSD1 appears to be a better target than SRD5A to slow abiraterone metabolism.

3βHSD1 is also involved in enzalutamide resistance. Enhanced steroidogenesis was observed in enzalutamide-resistant cell lines. Enzalutamide could still bind to ARs as an

Figure 4. BCA antagonizes 3βHSD1-related cancer development and enzalutamide resistance

(A) Structures of corylin, BCA, and daidzein.

(B) BCA inhibited DHEA conversion to AD. Cells were treated with [^{3}H]-DHEA and the indicated drugs. The percentages of DHEA and downstream metabolites were calculated. AD, androstenedione.

(C) BCA showed comparable inhibition to different isoforms of 3βHSD1. Plasmids expressing 3βHSD1 (367T) or 3βHSD1 (367N) isoforms were transfected in 293T cells, and the related cell lysates were used for a metabolism assay.

(D) Lineweaver-Burk plots of BCA inhibition of 3βHSD1 activity. Lysates of 293T cells expressing 3βHSD1 were incubated with BCA and DHEA.

(E) Effect of BCA on CYP17A activity. HEK 293 cells with stable CYP17A overexpression were treated with [^{3}H]-pregnenolone and the indicated drugs.

(F) Effect of BCA on SRD5A activity. LAPC4 cells were treated with [^{3}H]-AD and the indicated drugs.

(G) BCA suppressed DHEA regulation of AR protein abundance in VCaP and LNCaP cells. DHEA, 200 nM; DHT, 1 nM; BCA, 1 μM; Enz, 1 μM.

(H) BCA inhibited DHEA-induced cell growth. VCaP cells were treated with indicated drugs.

(I) BCA inhibited DHEA-induced VCaP xenograft growth. BCA, 30 mg/kg. Ctr group, n = 9; BCA group, n = 10.

(J) BCA and enzalutamide synergistically inhibited DHEA- but not DHT-induced gene expression in VCaP-Enz cells. ns, not significant.

(K) Corylin and enzalutamide synergistically inhibited DHEA- but not DHT-induced gene expression in VCaP-Enz cells. DHEA, 100 nM; DHT, 1 nM.

(L) BCA and enzalutamide synergistically inhibited DHEA- but not DHT-induced cell growth in VCaP-Enz cells. DHEA, 100 nM; DHT, 1 nM.

(M) Corylin and enzalutamide synergistically inhibited DHEA- but not DHT-induced cell growth in VCaP-Enz cells. DHEA, 200 nM; DHT, 1 nM.

(N) The combination of BCA and enzalutamide more effectively inhibited DHEA-induced xenograft growth than either drug alone. VCaP-Enz cells were used to create the xenograft. BCA, 30 mg/kg; Enz, 10 mg/kg. n = 9 for each group.

*p < 0.05; **p < 0.01. Student's t test. Results are presented as mean ± SD. Experiments were performed at least three times independently.

See also Figure S5.

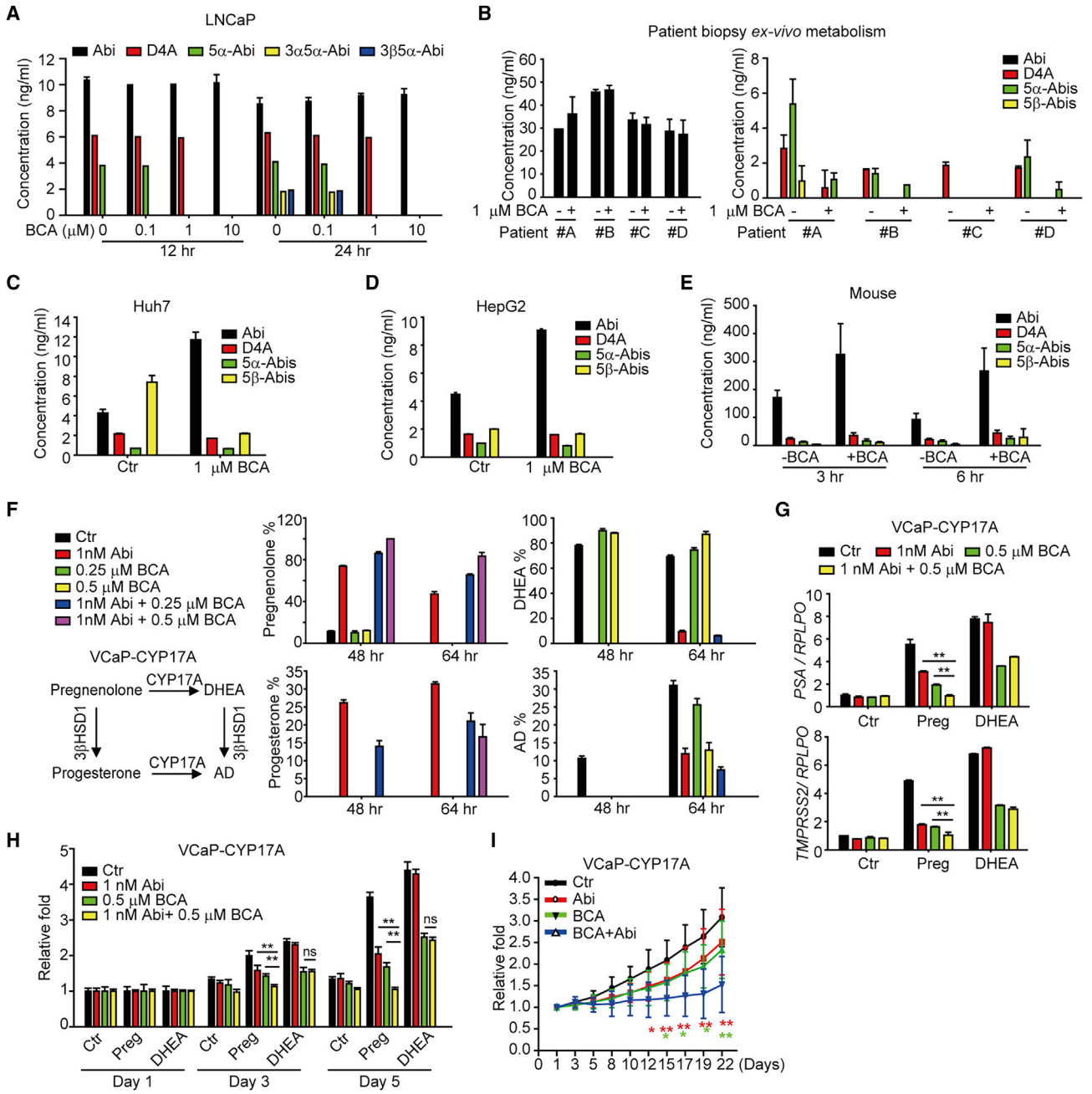

Figure 5. BCA regulates abiraterone metabolism to enhance the efficacy of abiraterone

(A) BCA regulated abiraterone metabolism in the LNCaP cell line. LNCaP cells were treated with 10 nM abiraterone, with or without BCA.

(B) BCA regulated abiraterone metabolism in patient biopsy tissues. Three fresh biopsy tissues were collected from each of 4 patients with localized prostate cancer (patients #A–D). Each biopsy sample was equally divided in 2 halves and treated with 100 nM abiraterone, with or without 1 μM BCA.

(C and D) BCA regulated abiraterone metabolism in Huh7 (C) and HepG2 (D) cells. Liver cells were treated with 100 nM abiraterone with or without 1 μM BCA for 24 h.

(E) BCA regulated abiraterone metabolism in mouse. Mice were treated with 50 mg/kg BCA and 0.5 mmol/kg abiraterone acetate. Blood samples were collected at the indicated time points.

(F) BCA and abiraterone inhibited pregnenolone metabolism. VCaP cells expressing CYP17A were treated with [^{3}H]-pregnenolone and the indicated drugs.

(G and H) BCA and abiraterone inhibited pregnenolone-induced AR signaling activity (G) and cell growth (H) more effectively. Pregnenolone, 100 nM; DHEA, 100 nM.

(I) BCA and abiraterone inhibited DHEA-induced xenograft growth more effectively than abiraterone alone. BCA, 50 mg/kg; abiraterone acetate, 0.1 mmol/kg. Ctr, n = 8; Abi, n = 7; BCA, n = 8; BCA + Abi, n = 9. Red *, Abi versus BCA + Abi; green *, BCA versus BCA + Abi.

*$p < 0.05$; **$p < 0.01$. Student's t test. Results are presented as mean ± SD. Experiments were performed at least three times independently.

See also Figure S6.

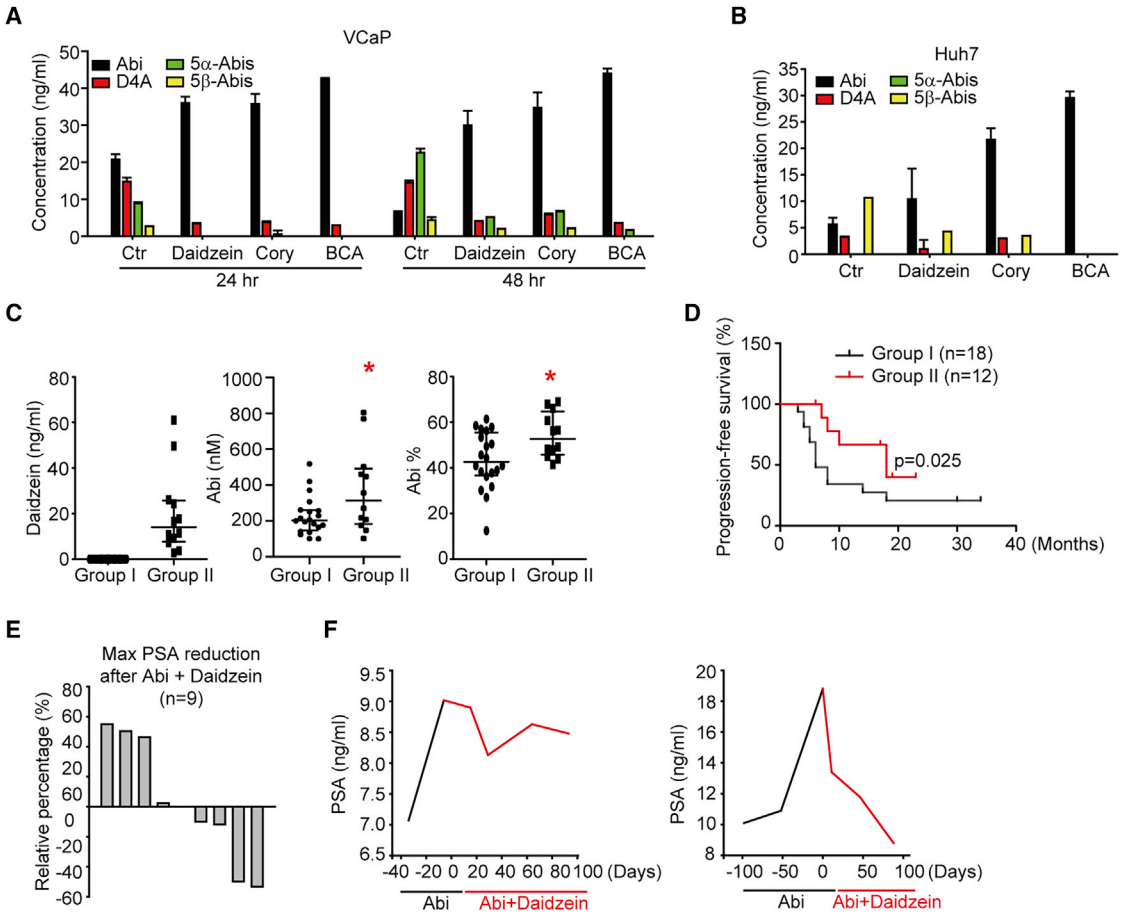

Figure 6. Daidzein enhances the clinical efficacy of abiraterone

(A) Daidzein regulated Abi metabolism in VCaP cells. Abi, 10 nM; BCA and its derivatives, 1 μM.

(B) Daidzein regulated Abi metabolism in Huh7 cells. Abi, 100 nM; BCA and its derivatives, 1 μM.

(C) Patients with detectable plasma daidzein had a higher concentration and relative percentage of plasma abiraterone. Group I, n = 20; group II, n = 12.

(D) Progression-free survival of patients with or without detectable plasma daidzein. Significance was calculated using the Gehan-Breslow-Wilcoxon test.

(E) Maximum PSA reduction after daidzein treatment in 9 patients with abiraterone resistance.

(F) PSA change in 2 patients before and after daidzein treatment.

*$p < 0.05$. Student's t test. Results are presented as mean ± SD. Experiments were performed at least three times independently.

See also Tables S3 and S4.

antagonist. However, 3βHSD1 activity facilitated the generation and accumulation of intracellular DHT to compete with enzalutamide. As a next generation of AR antagonist, enzalutamide still has weaker affinity for ARs than that of endogenous androgens. Potent 3βHSD1-mediated steroidogenesis has also been observed in patients with abiraterone resistance: biopsy samples collected from a patient with resistance showed recovered 3βHSD1 activity.[10] These results all support the importance of the androgen-AR axis after abiraterone or enzalutamide resistance.[9,50] Notably, long-term treatment of enzalutamide resulted in an increase of 3βHSD1 activity in VCaP cells, which also express ARv7, indicating the co-existence of multiple resistant mechanisms.

Persistent efforts have been made to discover inhibitors of 3βHSD1 for the management of multiple diseases.[23,40,51,52] Trilostane is a well-known 3βHSD1 inhibitor, but it activates AR directly.[53,54] D4A, a metabolite of abiraterone, potently inhibits 3βHSD1.[44] However, its clinical application is limited due to its rapid conversion to 5α-Abi.[33] Here, we showed that BCA is a potent non-steroidal 3βHSD1 inhibitor. The plasma concentration of daidzein, a derivative of BCA that less potently inhibits 3βHSD1, was associated with higher plasma abiraterone. Plasma concentrations of genistein and daidzein, originating from the daily diet, have been reported to be inversely correlated with the risk of prostate cancer in Japanese patients.[55] In our abiraterone-resistant patients, daidzein halted PSA increases in 5 patients and resulted in a maximum PSA reduction of more than 50% in 2 patients, highlighting the potential clinical application of BCA as a 3βHSD1 inhibitor. Previous investigations in rats found that BCA has low bioavailability (~4%) and is rapidly converted to genistein, which would hinder the efficacy of BCA in

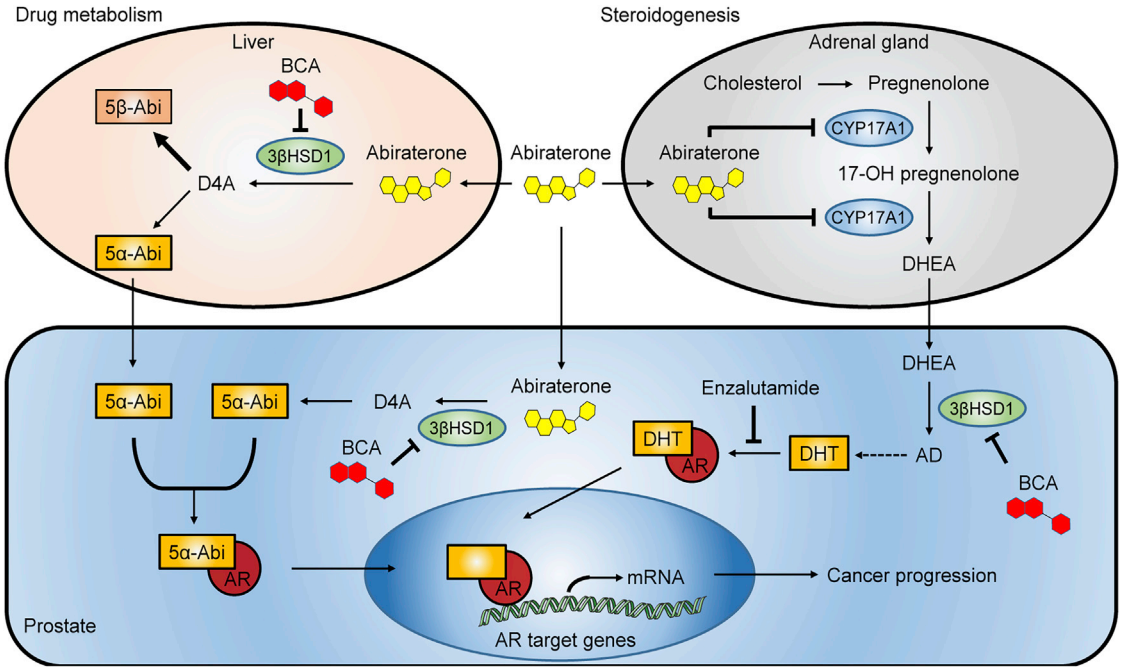

Figure 7. Schema of 3βHSD1 and BCA function in prostate cancer

The steroidogenic enzyme 3βHSD1 facilitates DHT generation from DHEA to impair the function of enzalutamide. 3βHSD1 also promotes abiraterone metabolism to accelerate drug clearance. BCA inhibits 3βHSD1 to overcome resistance to enzalutamide and abiraterone.

clinic.[56,57] Consequently, structural modification of BCA or a novel drug delivery system may be needed to improve the function of BCA in clinic.

In summary, we demonstrate that 3βHSD1 is essential in the development of resistance to abiraterone and enzalutamide. By targeting 3βHSD1, BCA and its derivatives inhibit prostate cancer development by simultaneous regulation of androgen and drug metabolism (Figure 7).

Limitations of the study

There are several limitations of this study. The major limitations were small sample size and patient selection (only Chinese patients were recruited for this investigation). Daidzein is used for the clinical research, and BCA, as the most potent 3βHSD1 inhibitor, is not available in clinic.

STAR★METHODS

Detailed methods are provided in the online version of this paper and include the following:

- KEY RESOURCES TABLE
- RESOURCE AVAILABILITY
  - Lead contact
  - Materials availability
  - Data and code availability
- EXPERIMENTAL MODEL AND SUBJECT DETAILS
  - Patient recruitment
  - Mouse xenograft studies
  - Cell lines
- METHOD DETAILS
  - Metabolism in cell line, biopsies, and mouse
  - Mass spectrometry
  - HPLC
  - Gene expression assay
  - AR competition assay
  - RNA-seq
  - GSEA analysis and ChIP-seq analysis
  - Cell proliferation assay
  - Pyrosequencing
- QUANTIFICATION AND STATISTICAL ANALYSIS

SUPPLEMENTAL INFORMATION

Supplemental information can be found online at https://doi.org/10.1016/j.xcrm.2022.100608.

ACKNOWLEDGMENTS

We thank our patients and their families. We thank the staff members (Zhuo Yang et al.) of the Chemical Biology Core Facility at the Shanghai Institute of Biochemistry and Cell Biology, staff members (Chao Peng et al.) of Mass Spectrometry at the National Facility for Protein in Shanghai (NFPS)/Shanghai Advanced Research Institute, and staff members (Pengyu Wang et al.) of the Bio-Med Big Data Center/Shanghai Institute of Nutrition and Health for support. This work is supported by the National Key R&D Program of China (2018YFA0508200), the National Natural Science Foundation of China (92157101, 81722033, and 81872075), the New Frontier Technology Joint Research Project of Shanghai Municipal Hospital (SHDC12019112), the Natural Science Foundation of Shanghai Municipal Science and Technology Committee (21ZR1458300), and a Prostate Cancer Foundation Young Investigator Award.

AUTHOR CONTRIBUTIONS

Conceptualization, Z.L. and S.H.; methodology, T.Y. and Y.G.; investigation, Z.M., T.Y., Y.G., Y.L., Z.H., D.H., Q.Z., X. Zhang, Q.T., X. Zhu, Y.Q., X.C., C.X., C.B., X.W., C.W., and D.W.; writing, Z.L., S.H., Z.M., and D.W.; funding acquisition, Z.L., D.W., and S.H.; resources, S.H. and D.W.; supervision, Z.L. and S.H.

DECLARATION OF INTERESTS

These authors declare no competing interests.

Received: December 8, 2021
Revised: February 27, 2022
Accepted: March 25, 2022
Published: April 20, 2022

REFERENCES

1. Xia, C., Dong, X., Li, H., Cao, M., Sun, D., He, S., Yang, F., Yan, X., Zhang, S., and Li, N. (2022). Cancer statistics in China and United States, 2022: profiles, trends, and determinants. Chin Med. J. (Engl) *135*, 584–590.
2. Siegel, R.L., Miller, K.D., Fuchs, H.E., and Jemal, A. (2022). Cancer statistics. CA Cancer J. Clin. *72*, 7–33.
3. Hou, Z., Huang, S., and Li, Z. (2021). Androgens in prostate cancer: a tale that never ends. Cancer Lett. *516*, 1–12.
4. de Bono, J.S., Logothetis, C.J., Molina, A., Fizazi, K., North, S., Chu, L., Chi, K.N., Jones, R.J., Goodman, O.B., Saad, F., et al. (2011). Abiraterone and increased survival in metastatic prostate cancer. N. Engl. J. Med. *364*, 1995–2005.
5. Scher, H.I., Fizazi, K., Saad, F., Taplin, M.E., Sternberg, C.N., Miller, K., de Wit, R., Mulders, P., Chi, K.N., Shore, N.D., et al. (2012). Increased survival with enzalutamide in prostate cancer after chemotherapy. N. Engl. J. Med. *367*, 1187–1197.
6. Beltran, H., Rickman, D.S., Park, K., Chae, S.S., Sboner, A., MacDonald, T.Y., Wang, Y., Sheikh, K.L., Terry, S., Tagawa, S.T., et al. (2011). Molecular characterization of neuroendocrine prostate cancer and identification of new drug targets. Cancer Discov. *1*, 487–495.
7. Dardenne, E., Beltran, H., Benelli, M., Gayvert, K., Berger, A., Puca, L., Cyrta, J., Sboner, A., Noorzad, Z., MacDonald, T., et al. (2016). N-myc induces an EZH2-mediated transcriptional program driving neuroendocrine prostate cancer. Cancer Cell *30*, 563–577.
8. Davies, A.H., Beltran, H., and Zoubeidi, A. (2018). Cellular plasticity and the neuroendocrine phenotype in prostate cancer. Nat. Rev. Urol. *15*, 271–286.
9. Efstathiou, E., Titus, M., Wen, S., Hoang, A., Karlou, M., Ashe, R., Tu, S.M., Aparicio, A., Troncoso, P., Mohler, J., et al. (2015). Molecular characterization of enzalutamide-treated bone metastatic castration-resistant prostate cancer. Eur. Urol. *67*, 53–60.
10. Hou, Z., Yang, T., Mei, Z., Zhang, S., Gao, Y., Chen, X., Tan, Q., Zhu, X., Xu, C., Lian, J., et al. (2021). Tracing steroidogenesis in prostate biopsy samples to unveil prostate tissue androgen metabolism characteristics and potential clinical application. J. Steroid Biochem. Mol. Biol. *210*, 105859.
11. Schrader, A.J., Boegemann, M., Ohlmann, C.H., Schnoeller, T.J., Krabbe, L.M., Hajili, T., Jentzmik, F., Stoeckle, M., Schrader, M., Herrmann, E., et al. (2014). Enzalutamide in castration-resistant prostate cancer patients progressing after docetaxel and abiraterone. Eur. Urol. *65*, 30–36.
12. Brasso, K., Thomsen, F.B., Schrader, A.J., Schmid, S.C., Lorente, D., Retz, M., Merseburger, A.S., von Klot, C.A., Boegemann, M., and de Bono, J. (2015). Enzalutamide antitumour activity against metastatic castration-resistant prostate cancer previously treated with docetaxel and abiraterone: a multicentre analysis. Eur. Urol. *68*, 317–324.
13. Francini, E., Petrioli, R., and Roviello, G. (2014). No clear evidence of a clinical benefit of a sequential therapy regimen with abiraterone acetate and enzalutamide. Expert Rev. Anticancer Ther. *14*, 1135–1140.
14. Watson, P.A., Arora, V.K., and Sawyers, C.L. (2015). Emerging mechanisms of resistance to androgen receptor inhibitors in prostate cancer. Nat. Rev. Cancer *15*, 701–711.
15. Khalaf, D.J., Aragon, I.M., Annala, M., Lozano, R., Taavitsainen, S., Lorente, D., Finch, D., Romero-Laorden, N., Vergidis, J., Cendon, Y., et al. (2020). HSD3B1 (1245A>C) germline variant and clinical outcomes in metastatic castration-resistant prostate cancer patients treated with abiraterone and enzalutamide: results from two prospective studies. Ann. Oncol. *31*, 1186–1197.
16. Lu, C., Terbuch, A., Dolling, D., Yu, J., Wang, H., Chen, Y., Fountain, J., Bertan, C., Sharp, A., Carreira, S., et al. (2020). Treatment with abiraterone and enzalutamide does not overcome poor outcome from metastatic castration-resistant prostate cancer in men with the germline homozygous HSD3B1 c.1245C genotype. Ann. Oncol. *31*, 1178–1185.
17. Bolger, A.M., Lohse, M., and Usadel, B. (2014). Trimmomatic: a flexible trimmer for Illumina sequence data. Bioinformatics *30*, 2114–2120.
18. Pertea, M., Kim, D., Pertea, G.M., Leek, J.T., and Salzberg, S.L. (2016). Transcript-level expression analysis of RNA-seq experiments with HISAT, StringTie and Ballgown. Nat. Protoc. *11*, 1650–1667.
19. Li, H., Handsaker, B., Wysoker, A., Fennell, T., Ruan, J., Homer, N., Marth, G., Abecasis, G., and Durbin, R. (2009). The sequence alignment/map format and SAMtools. Bioinformatics *25*, 2078–2079.
20. Anders, S., Pyl, P.T., and Huber, W. (2015). HTSeq–a Python framework to work with high-throughput sequencing data. Bioinformatics *31*, 166–169.
21. Love, M.I., Huber, W., and Anders, S. (2014). Moderated estimation of fold change and dispersion for RNA-seq data with DESeq2. Genome Biol. *15*, 550.
22. Subramanian, A., Tamayo, P., Mootha, V.K., Mukherjee, S., Ebert, B.L., Gillette, M.A., Paulovich, A., Pomeroy, S.L., Golub, T.R., Lander, E.S., et al. (2005). Gene set enrichment analysis: a knowledge-based approach for interpreting genome-wide expression profiles. Proc. Natl. Acad. Sci. U S A *102*, 15545–15550.
23. Chang, K.H., Li, R., Kuri, B., Lotan, Y., Roehrborn, C., Liu, J., Vessella, R., Nelson, P., Kapur, P., Guo, X., et al. (2013). A gain-of-function mutation in DHT synthesis in castration-resistant prostate cancer. Cell *154*, 1074–1084.
24. Asangani, I.A., Dommeti, V.L., Wang, X., Malik, R., Cieslik, M., Yang, R., Escara-Wilke, J., Wilder-Romans, K., Dhanireddy, S., Engelke, C., et al. (2014). Therapeutic targeting of BET bromodomain proteins in castration-resistant prostate cancer. Nature *510*, 278–282.
25. Massie, C.E., Lynch, A., Ramos-Montoya, A., Boren, J., Stark, R., Fazli, L., Warren, A., Scott, H., Madhu, B., Sharma, N., et al. (2011). The androgen receptor fuels prostate cancer by regulating central metabolism and biosynthesis. EMBO J. *30*, 2719–2733.
26. Takayama, K., Suzuki, T., Tsutsumi, S., Fujimura, T., Urano, T., Takahashi, S., Homma, Y., Aburatani, H., Inoue, S., et al. (2015). RUNX1, an androgen- and EZH2-regulated gene, has differential roles in AR-dependent and -independent prostate cancer. Oncotarget *6*, 2263–2276.
27. Zhao, J.C., Fong, K.W., Jin, H.J., Yang, Y.A., Kim, J., and Yu, J. (2016). FOXA1 acts upstream of GATA2 and AR in hormonal regulation of gene expression. Oncogene *35*, 4335–4344.
28. Pomerantz, M.M., Li, F., Takeda, D.Y., Lenci, R., Chonkar, A., Chabot, M., Cejas, P., Vazquez, F., Cook, J., Shivdasani, R.A., et al. (2015). The androgen receptor cistrome is extensively reprogrammed in human prostate tumorigenesis. Nat. Genet. *47*, 1346–1351.
29. Taylor, B.S., Schultz, N., Hieronymus, H., Gopalan, A., Xiao, Y., Carver, B.S., Arora, V.K., Kaushik, P., Cerami, E., Reva, B., et al. (2010). Integrative genomic profiling of human prostate cancer. Cancer Cell *18*, 11–22.
30. Tran, C., Ouk, S., Clegg, N.J., Chen, Y., Watson, P.A., Arora, V., Wongvipat, J., Smith-Jones, P.M., Yoo, D., Kwon, A., et al. (2009). Development of

a second-generation antiandrogen for treatment of advanced prostate cancer. Science *324*, 787–790.

31. Thomas, L., and Sharifi, N. (2020). Germline HSD3B1 genetics and prostate cancer outcomes. Urology *145*, 13–21.
32. Cao, Y., Li, L., Xu, M., Feng, Z., Sun, X., Lu, J., Xu, Y., Du, P., Wang, T., Hu, R., et al. (2020). The ChinaMAP analytics of deep whole genome sequences in 10,588 individuals. Cell Res. *30*, 717–731.
33. Li, Z., Alyamani, M., Li, J., Rogacki, K., Abazeed, M., Upadhyay, S.K., Balk, S.P., Taplin, M.E., Auchus, R.J., and Sharifi, N. (2016). Redirecting abiraterone metabolism to fine-tune prostate cancer anti-androgen therapy. Nature *533*, 547–551.
34. Alyamani, M., Emamekhoo, H., Park, S., Taylor, J., Almassi, N., Upadhyay, S., Tyler, A., Berk, M.P., Hu, B., Hwang, T.H., et al. (2018). HSD3B1(1245A>C) variant regulates dueling abiraterone metabolite effects in prostate cancer. J. Clin. Invest. *128*, 3333–3340.
35. Zheng, Z.G., Zhang, X., Liu, X.X., Jin, X.X., Dai, L., Cheng, H.M., Jing, D., Thu, P.M., Zhang, M., Li, H., et al. (2019). Inhibition of HSP90beta improves lipid disorders by promoting mature SREBPs degradation via the ubiquitin-proteasome system. Theranostics *9*, 5769–5783.
36. Hou, Z., Huang, S., Mei, Z., Chen, L., Guo, J., Gao, Y., Zhuang, Q., Zhang, X., Tan, Q., Yang, T., et al. (2022). Inhibiting 3βHSD1 to eliminate the oncogenic effects of progesterone in prostate cancer. Cell Rep. Med. *3*, 100561.
37. Chaturvedi, A.P., and Dehm, S.M. (2019). Androgen receptor dependence. Adv. Exp. Med. Biol. *1210*, 333–350.
38. McKay, R.R., Werner, L., Mostaghel, E.A., Lis, R., Voznesensky, O., Zhang, Z., Marck, B.T., Matsumoto, A.M., Domachevsky, L., Zukotynski, K.A., et al. (2017). A phase II trial of abiraterone combined with dutasteride for men with metastatic castration-resistant prostate cancer. Clin. Cancer Res. *23*, 935–945.
39. Andriole, G.L., Bostwick, D.G., Brawley, O.W., Gomella, L.G., Marberger, M., Montorsi, F., Pettaway, C.A., Tammela, T.L., Teloken, C., Tindall, D.J., et al. (2010). Effect of dutasteride on the risk of prostate cancer. N. Engl. J. Med. *362*, 1192–1202.
40. Hearn, J.W., AbuAli, G., Reichard, C.A., Reddy, C.A., Magi-Galluzzi, C., Chang, K.H., Carlson, R., Rangel, L., Reagan, K., Davis, B.J., et al. (2016). HSD3B1 and resistance to androgen-deprivation therapy in prostate cancer: a retrospective, multicohort study. Lancet Oncol. *17*, 1435–1444.
41. Agarwal, N., Hahn, A.W., Gill, D.M., Farnham, J.M., Poole, A.I., and Cannon-Albright, L. (2017). Independent validation of effect of HSD3B1 genotype on response to androgen-deprivation therapy in prostate cancer. JAMA Oncol. *3*, 856–857.
42. Shiota, M., Narita, S., Akamatsu, S., Fujimoto, N., Sumiyoshi, T., Fujiwara, M., Uchiumi, T., Habuchi, T., Ogawa, O., and Eto, M. (2019). Association of missense polymorphism in HSD3B1 with outcomes among men with prostate cancer treated with androgen-deprivation therapy or abiraterone. JAMA Netw. Open *2*, e190115.
43. Hahn, A.W., Gill, D.M., Nussenzveig, R.H., Poole, A., Farnham, J., Cannon-Albright, L., and Agarwal, N. (2018). Germline variant in HSD3B1 (1245 A > C) and response to abiraterone acetate plus prednisone in men with new-onset metastatic castration-resistant prostate cancer. Clin. Genitourin Cancer *16*, 288–292.
44. Li, Z., Bishop, A.C., Alyamani, M., Garcia, J.A., Dreicer, R., Bunch, D., Liu, J., Upadhyay, S.K., Auchus, R.J., and Sharifi, N. (2015). Conversion of abiraterone to D4A drives anti-tumour activity in prostate cancer. Nature *523*, 347–351.
45. Szmulewitz, R.Z., Peer, C.J., Ibraheem, A., Martinez, E., Kozloff, M.F., Carthon, B., Harvey, R.D., Fishkin, P., Yong, W.P., Chiong, E., et al. (2018). Prospective international randomized phase II study of low-dose abiraterone with food versus standard dose abiraterone in castration-resistant prostate cancer. J. Clin. Oncol. *36*, 1389–1395.
46. Attard, G., Reid, A.H., Yap, T.A., Raynaud, F., Dowsett, M., Settatree, S., Barrett, M., Parker, C., Martins, V., Folkerd, E., et al. (2008). Phase I clinical trial of a selective inhibitor of CYP17, abiraterone acetate, confirms that castration-resistant prostate cancer commonly remains hormone driven. J. Clin. Oncol. *26*, 4563–4571.
47. van Nuland, M., Groenland, S.L., Bergman, A.M., Steeghs, N., Rosing, H., Venekamp, N., Huitema, A.D.R., Beijnen, J.H., et al. (2019). Exposure-response analyses of abiraterone and its metabolites in real-world patients with metastatic castration-resistant prostate cancer. Prostate Cancer Prostatic Dis. *23*, 244–251.
48. Carton, E., Noe, G., Huillard, O., Golmard, L., Giroux, J., Cessot, A., Saidu, N., Peyromaure, M., Zerbib, M., Narjoz, C., et al. (2017). Relation between plasma trough concentration of abiraterone and prostate-specific antigen response in metastatic castration-resistant prostate cancer patients. Eur. J. Cancer *72*, 54–61.
49. Friedlander, T.W., Graff, J.N., Zejnullahu, K., Anantharaman, A., Zhang, L., Paz, R., Premasekharan, G., Russell, C., Huang, Y., Kim, W., et al. (2017). High-dose abiraterone acetate in men with castration resistant prostate cancer. Clin. Genitourin Cancer *15*, 733–741.e1.
50. Liu, C., Yang, J.C., Armstrong, C.M., Lou, W., Liu, L., Qiu, X., Zou, B., Lombard, A.P., D'Abronzo, L.S., Evans, C.P., et al. (2019). AKR1C3 promotes AR-V7 protein stabilization and confers resistance to AR-targeted therapies in advanced prostate cancer. Mol. Cancer Ther. *18*, 1875–1886.
51. Almassi, N., Reichard, C., Li, J., Russell, C., Perry, J., Ryan, C.J., Friedlander, T., Sharifi, N., et al. (2018). HSD3B1 and response to a nonsteroidal CYP17A1 inhibitor in castration-resistant prostate cancer. JAMA Oncol. *4*, 554–557.
52. Hearn, J.W.D., Xie, W., Nakabayashi, M., Almassi, N., Reichard, C.A., Pomerantz, M., Kantoff, P.W., Sharifi, N., et al. (2018). Association of HSD3B1 genotype with response to androgen-deprivation therapy for biochemical recurrence after radiotherapy for localized prostate cancer. JAMA Oncol. *4*, 558–562.
53. Pham, J.H., Will, C.M., Mack, V.L., Halbert, M., Conner, E.A., Bucholtz, K.M., and Thomas, J.L. (2017). Structure-function relationships for the selective inhibition of human 3beta-hydroxysteroid dehydrogenase type 1 by a novel androgen analog. J. Steroid Biochem. Mol. Biol. *174*, 257–264.
54. Evaul, K., Li, R., Papari-Zareei, M., Auchus, R.J., and Sharifi, N. (2010). 3beta-hydroxysteroid dehydrogenase is a possible pharmacological target in the treatment of castration-resistant prostate cancer. Endocrinology *151*, 3514–3520.
55. Kurahashi, N., Iwasaki, M., Inoue, M., Sasazuki, S., and Tsugane, S. (2008). Plasma isoflavones and subsequent risk of prostate cancer in a nested case-control study: the Japan Public Health Center. J. Clin. Oncol. *26*, 5923–5929.
56. Moon, Y.J., Sagawa, K., Frederick, K., Zhang, S., and Morris, M.E. (2006). Pharmacokinetics and bioavailability of the isoflavone biochanin A in rats. AAPS J. *8*, E433–E442.
57. Mallis, L.M., Sarkahian, A.B., Harris, H.A., Zhang, M., and MCconnell, O. (2003). Determination of rat oral bioavailability of soy-derived phytoestrogens using an automated on-column extraction procedure and electrospray tandem mass spectrometry. J. Chromatogr. B Analyt Technol. Biomed. Life Sci. *796*, 71–86.
58. Lian, J.P., Gao, Y.Y., Tang, J.J., Wu, D.L., Lian, J.P., Huang, S.S., Gao, Y.Y., and Tang, J.J. (2020). Response of prostate cancer to addition of dutasteride after progression on abiraterone. Asian J. Androl. *23*, 222–223.
59. Scher, H.I., Halabi, S., Tannock, I., Morris, M., Sternberg, C.N., Carducci, M.A., Eisenberger, M.A., Higano, C., Bubley, G.J., Dreicer, R., et al. (2008). Design and end points of clinical trials for patients with progressive prostate cancer and castrate levels of testosterone: recommendations of the Prostate Cancer Clinical Trials Working Group. J. Clin. Oncol. *26*, 1148–1159.
60. Gao, X., Dai, C., Huang, S., Tang, J., Chen, G., Li, J., Zhu, Z., Zhu, X., Zhou, S., Gao, Y., et al. (2019). Functional silencing of HSD17B2 in prostate cancer promotes disease progression. Clin. Cancer Res. *25*, 1291–1301.

STAR★METHODS

KEY RESOURCES TABLE

REAGENT or RESOURCE	SOURCE	IDENTIFIER
Antibodies		
mouse anti-AR	Santa Cruz Biotechnology	Cat#sc-7305
mouse anti-3βHSD1	Abcam	Cat#ab55268
mouse anti-FLAG	Sigma	Cat#F1804
rabbit anti-β-actin	Abclonal	Cat#AC026
mouse anti-Lamin B1	Proteintech	Cat#66095
mouse anti-Tubulin	Proteintech	Cat#66031
Daidzein	MedChem Express	Cat#HY-N0019; Cas#486-66-8
Bacterial and virus strains		
DH5α	TransGen Biotech	Cat#P1050425
BL21	TIANGEN	Cat#CB105
BL21 (DE3)	TIANGEN	Cat#CB108
Biological samples		
Patient plasma	Tongji Hospital (Shanghai)	Tables S1–S4
Patient biopsies	Tongji Hospital (Shanghai)	Hou et al., 2021[10]
Chemicals, peptides, and recombinant proteins		
RPMI-1640 Medium, with L-glutamine and sodium bicarbonate	Sigma-Aldrich	Cat#R8758
RPMI-1640 Medium, without L-glutamine and phenol red	Sigma-Aldrich	Cat#R7509
DMEM - high glucose	Sigma-Aldrich	Cat#D7777
DMEM, without glucose, L-glutamine, phenol red, sodium pyruvate and sodium bicarbonate	Sigma-Aldrich	Cat#D5030
IMDM	Sigma-Aldrich	Cat#I3390
IMDM, without Gentamicin Sulfate and phenol red	Sigma-Aldrich	Cat#A10488
Trypsin-EDTA solution	Sigma-Aldrich	Cat#T4049
Fetal Bovine Serum	Lonsera	Cat#S711-001S
Charcoal stripped FBS	Lonsera	Cat#S883811
L-Glutamine solution	Sigma-Aldrich	Cat#G7513
Sodium pyruvate	Sigma-Aldrich	Cat#11360070
Lipofectamine 3000	Invitrogen	Cat#L3000-015
Lipofectamine RNAiMAX	Invitrogen	Cat#13778150
Puromycin	GIBCO	Cat#A1113802
G418, Geneticin	GIBCO	Cat#10131035
Pregnenolone	Steraloids Inc.	Cat#Q5500-000; Cas#145-13-1
Progesterone	Steraloids Inc	Cat#Q2600-000; Cas#57-83-0
Doxycycline hyclate	Sigma-Aldrich	Cat#10592-13-9
Polyethylenimine	Sigma-Aldrich	Cat#408727
Dihydrotestosterone (DHT)	MedChem Express	Cas#521-18-6; Cas#521-18-6
Dehydroepiandrosterone (DHEA)	Steraloids Inc	Cat#A8500-000; Cas#53-43-0
Biochanin A(BCA)	MedChem Express	Cat#HY-14595; Cas#491-80-5
Corylin	MedChem Express	Cat#HY-N0236; Cas#53947-92-5
Enzalutimide	Shanghai Forever Synthesis Co	Cas#915087-33-1
Abiraterone	Shanghai Forever Synthesis Co	Cas#154229-19-3

(*Continued on next page*)

Continued

REAGENT or RESOURCE	SOURCE	IDENTIFIER
Cortisol	Steraloids Inc	Cas#50-23-7
R1881	Meilunbio	Cas#965-93-5
D4A	Shanghai Forever Synthesis Co	N/A
Protease inhibitor cocktails	MedChem Express	Cat#HY-K0011
Poly-DL-ornithine	Sigma-Aldrich	Cat#P3655-1G
Pregnenolone pellets	EZBioscience	N/A
DHEA pellets	EZBioscience	N/A
Ethyl alcohol	Thermo Fisher Scientific	Cat#AC 615095000
Corning® Matrigel® Basement Membrane Matrix, *LDEV-Free	BD biocoat (Corning)	Cat#354234
[^{3}H]-DHEA	PerkinElmer	NET 814001MC
[^{3}H]-AD	PerkinElmer	NET 926005MC
[^{3}H]-Pregnenolone	PerkinElmer	NET 039001MC
[^{3}H]-R1881	PerkinElmer	NET 590250VC
[^{3}H]-Progesterone	PerkinElmer	NET 381
Methanol	Thermo Fisher Scientific	Cat#A454K4
Ethyl acetate	Sigma-Aldrich	Cat#34858-4L
Iso octane	Thermo Fisher Scientific	Cat#03014
Liquiscint scintillation cocktail	Thermo Fisher Scientific	Cat#5089990170
Tert-butyl methyl ether	Thermo Fisher Scientific	Cat#AC 389050025
TRIzol reagent	Thermo Fisher Scientific	Cat#15596026
G418	Thermo Fisher	Cat#10131035
Puromycin	Invitrogen-Gibco	Cat#A1113803
Matrigel	Corning	Cat#354234
Critical commercial assays		
Cell Counting Kit-8	Beyotime	Cat#C0038
Cell to cDNA Kit	EZBioscience	Cat#B0003
2x SYBR Green qPCR master mix	EZBioscience	Cat#A0001-R2
Pierce BCA Protein Assay Kit	Thermal Fisher Scientific	Cat#23225
Pierce ECL Western Blotting Substrate	Thermal Fisher Scientific	Cat#32209
KOD Hot Start DNA Polymerase	Merck	Cat#71086-3
Glo Lysis Buffer, 1X	Promega	Cat#E266A
Bright-Glo™ Luciferase Assay System	Promega	Cat#E2160
VAHTS™ mRNA-seq V3 Library Prep Kit for Illumina	Vazyme	Cat#NR611
VAHTS™ RNA Adapters set3 - set6 for Illumina	Vazyme	Cat#N809/N810/N811/N812
HiScript II Q RT SuperMix for qPCR (+gDNA wiper)	Vazyme	Cat#R223-01
ClonExpress II One Step Cloning Kit	Vazyme	Cat#C112-01
Deposited data		
Raw sequencing data	This paper	OEP000587
Experimental models: Cell lines		
LNCaP	ATCC	CRL-1740
VCaP	Dr. Jun Qin (SINH, China)	N/A
C4-2	ATCC	CRL-3314
LAPC4	Dr. Charles Sawyers (MSKCC, USA)	N/A
PC3	ATCC	CRL-1435
DU145	ATCC	HTB-81

(*Continued on next page*)

Continued

REAGENT or RESOURCE	SOURCE	IDENTIFIER
HEK293T	ATCC	CRL-3216
HEK293	ATCC	CRL-1573
Huh7	Cell Bank/Stem Cell bank, CAS	N/A
HepG2	Dr. Lijian Hui (SIBCB, Shanghai, China)	N/A
VCaP-Ctr	This paper	N/A
VCaP-Enz	This paper	N/A
LNCaP-Ctr	This paper	N/A
LNCaP-Enz-1uM	This paper	N/A
LNCaP-Enz-10uM	This paper	N/A
Huh7-Ctr	This paper	N/A
Huh7-Abi	This paper	N/A
VCaP-pLVX-*HSD3B1*	This paper	N/A
VCaP-CYP17A	This paper	N/A
Experimental models: Organisms/strains		
Mouse: NOD/SCID	Shanghai Lingchang Biotechnology	N/A
Oligonucleotides		
Primers for q-PCR or Clone	Table S5	N/A
Recombinant DNA		
pLVX-Tight-Puro (TetOn)	Clonetech	Cat#632162
pCDH-CMV-MCS-EF1-Puro	Biofeng	Cat#CD500B
Software and algorithms		
FastQC v0.11.7	Babraham Bioinformatics Institute	https://www.bioinformatics.babraham.ac.uk/projects/fastqc/
Trimmomatic v0.36-5	Bolger et al., 2014[17]	http://www.usadellab.org/cms/?page=trimmomatic
HISAT2 v2.2.1.0	Pertea et al., 2016[18]	http://ccb.jhu.edu/software/hisat2/index.shtml
Samtools	Li et al., 2009[19]	http://samtools.sourceforge.net/
HTSeq v.0.11.1	Anders et al., 2015[20]	https://htseq.readthedocs.io/en/release_0.9.1/
R v3.4.1	R Core Team	https://www.r-project.org/
R Studio	RStudio Team	https://www.rstudio.com/
DESeq2 v1.24.0	Love et al., 2014[21]	https://bioconductor.org/packages/release/bioc/html/DESeq2.html
Gene Set Enrichment Analysis v3.0	Subramanian et al., 2005[22]	https://www.gsea-msigdb.org/gsea/index.jsp

RESOURCE AVAILABILITY

Lead contact

Further information and request for resources and reagents should be directed to and will be fulfilled by the Lead Contact, Dr. Zhenfei Li (zhenfei.li@sibcb.ac.cn).

Materials availability

The plasmids, antibodies, stable cell lines and chemical compounds generated in this study have not been deposited to any repositories yet, however, these materials would be available from the Lead Contact without restriction.

Data and code availability

All RNA-seq data generated during this study have been deposited in the National Omics Data Encyclopedia/NODE (https://www.biosino.org/node) under the accession number OEP000587. This paper does not report original code. Any additional information required to reanalyze the data reported in this work paper is available from the Lead Contact upon request.

EXPERIMENTAL MODEL AND SUBJECT DETAILS

Patient recruitment

Plasma samples were collected from four different patient cohorts. All patients provided written informed consent, and all studies were approved by the local institutional review board. For each group, plasma samples were collected 3 h after abiraterone administration, according to the pharmacokinetics of abiraterone metabolism.[34] Plasma concentrations of abiraterone and its metabolites were determined with liquid chromatography-tandem mass spectrometry (LC-MS) as described previously.[58] The percentage of each metabolite was calculated as follows: metabolite/ (abiraterone + abiraterone metabolites) × 100%.

One group (n = 11) consisted of patients with CRPC undergoing abiraterone treatment (abiraterone, 1000 mg/day; prednisone, 5 BID) at Tongji Hospital (Shanghai, China) per a protocol approved by the institutional review board (ID: 2018009) (Table S1). Abiraterone resistance was determined based on the Prostate Cancer Working Group (PCWG) 2 guidelines.[59] Sequential plasma samples were collected from 11 mCRPC patients to trace alterations in abiraterone metabolism as disease progressed. A decrease of more than 25% from the abiraterone peak concentration, which was confirmed by a second value 3 or more weeks later, was recognized as a decline in plasma abiraterone concentration.

The second cohort consisted of patients (n = 19) who were enrolled and completed treatment in a single-arm, non-randomized clinical trial (ChiCTR1800015510; ID: 2018-LCYJ-003) investigating the clinical efficacy and limitations of dutasteride-regulated abiraterone metabolism in abiraterone-resistant patients with mCRPC (Table S2). Patients were treated with dutasteride (0.5 mg/day), abiraterone (1000 mg/day) and prednisone (5 mg twice daily). The primary outcome was progression-free survival as assessed by PSA level (PSA-PFS). Twenty-two patients (median age, 75 years) were enrolled, and 19 patients completed the treatment with a median follow-up of 4.0 months (3-18 months).

In the third cohort, plasma samples were collected from mCRPC patients (n = 32) receiving abiraterone treatment for at least 3 months at Tongji Hospital Shanghai from November 2017 to May 2019 (ID: 2018009) (Table S3). The plasma concentration of abiraterone and daidzein was determined with LC-MS.

Lastly, a single arm, non-blinded clinic trial (ChiCTR2000034019; ID: 2019080; Table S4) in June 2020 started enrollment of patients with abiraterone-resistant metastatic CRPC (mCRPC) to evaluate the safety and clinical efficacy of the combination of abiraterone and daidzein. Signed informed consents were collected. Patients were treated with daidzein (50 mg Bid), abiraterone (1000 mg/day), and prednisone (5 mg twice daily).

Mouse xenograft studies

Male B-NDG® (B-NDG) mice (B: Biocytogen; N: NOD background; D: DNAPK (Prkdc) null; G: IL2rgknockout) mice (aged 4 to 6 weeks) were obtained from Beijing Biocytogen. All mouse studies were conducted under a protocol approved by the Institutional Animal Care and Use Committee. Cells (1×10^7 cells) were implanted subcutaneously into the right flank of the intact mice with Matrigel (Corning, #354234). Mice were castrated and implanted with DHEA sustained-released pellets (EZBioscience, China) and randomly assigned into different groups when the xenografts reached approximately 200 mm^3 (length × width × width × 0.5). Stratified randomization was applied. Mice were first separated into different groups, according to the tumor size. Groups were then randomly assigned with different treatments. Tumor growth was measured every 2-3 days with a caliper. Student t test was used for significance calculation. *, $p < 0.05$; **, $p < 0.01$.

Xenograft tissues harvested from mice at the endpoint were homogenized in 1x RIPA buffer containing 10 μM MG132 and EDTA-free protease inhibitor cocktail via OMNI Bead Ruptor Elite (OMNI international, USA). The homogenate were further clarified by sonication and centrifugation before ready for western blot detection.

Cell lines

LNCaP and HEK 293T cells were purchased from the American Type Culture Collection (Manassas, VA) and maintained in RPMI-1640 (LNCaP) or DMEM (HEK 293T) with 10% FBS (ExCell Bio, China). VCaP was kindly provided by Dr. Jun Qin (SINH, Shanghai, China). Huh7 were purchased from Cell Bank/Stem Cell bank, the Chinese Academy of Sciences. HePG2 cells was kindly provided by Lijian Hui (SIBCB, CAS). All experiments with LNCaP and VCaP were done in plates coated with poly-DL-ornithine (Sigma-Aldrich, St. Louis, MO). Cell lines were authenticated by Hybribio (Guangzhou, China) and determined to be mycoplasma free with primers 5′-GGGAGCAAACAGGATTAGATACCCT-3′ and 5′-TGCACCATCTGT CACTCTGTTAACCTC-3′. The following primary antibodies were used: anti-3βHSD1 (Abcam, #ab55268) and anti-β-actin (ABclonal, #AC026).

VCaP cells were treated with ethanol or 1 μM Enz for 3 months to generate VCaP-Ctr and VCaP-Enz cells, respectively. VCaP cells were abruptly exposed to medium containing 1 μM Enz. LNCaP cells were treated with ethanol, 1 μM Enz, and 10 μM Enz for one month to generate LNCaP-Ctr, LNCaP-1 μM, and LNCaP-10 μM Enz cells.

METHOD DETAILS

Metabolism in cell line, biopsies, and mouse

For cell line metabolism, cells were treated with Abi (10 nM for LNCaP or 100 nM for Huh7 and HepG2) and BCA (1 μM) at 37 °C. Medium were collected at the indicated time and analyzed by LC-MS. Results represented the mean and sd value from one representative experiment. Experiments were performed in biology triplicate and repeated at least three times independently.

For biopsy tissue metabolism in Figure 1H, nine biopsy samples were collected from four patients with localized prostate cancer and cultured *ex vivo* transiently as previously reported.[10] Each biopsy was divided equally to two part. One was treat with 10 μM enzalutamide +100 nM DHEA *ex vivo* for one week and the other with ethanol with 100 nM DHEA. Then, biopsy samples were all treated with [^{3}H]-DHEA for steroidogenesis analysis. For biopsy tissue metabolism in Figure 5B, biopsy samples were collected from four patients with localized prostate cancer (three biopsy tissues/patient) with signed consent following a protocol approved by the institutional review board. Each biopsy tissue was divided equally with the same weight into two groups. One group was treated with 100 nM Abi and the other was treated with 100 nM Abi +1 μM BCA. Medium was collected after incubation for the indicated time and analyzed by LC-MS. The collection of biopsy samples met relevant ethical standards and was approved by the Ethics Committee of Tongji Hospital. All patients signed informed consent form.

For Abi metabolism in mouse, mice were randomly divided into two groups, Abi acetate (n = 5 mice, 0.5 mmol/kg) and Abi acetate + BCA (n = 4 mice; Abi, 0.5 mmol/kg; BCA, 50 mg/kg) were administrated through intraperitoneal injection. Plasma samples were collected from orbital veins at the indicated time and analyzed by LC-MS.

Mass spectrometry

A liquid chromatography-mass spectrometry (LC-MS) method was established to detect all 8 abiraterone metabolites and daidzein at the same time.[58] The extract of plasma samples were analyzed on a high-performance liquid chromatography station (Agilent, Santa Clara, CA) equipped with G4204A pumps, a G1367E auto-sampler, a G1316A column oven and a triple quadrupole 6490 (Agilent, Santa Clara, CA). Separation of drug metabolites was achieved using an Eclipse plus C18 RRHD analytical column 3.0 mm × 50 mm, 1.8 μM (Agilent, Santa Clara, CA) at 40°C with an isocratic mobile phase consisting of 70% buffer A (0.1% formic acid in methanol: water, 60:40) and 30% buffer B (0.1% formic acid in acetonitrile: water, 60:40), at a flow rate of 0.2 mL/min. The injection volume was 10 μL and sample injection was performed with the auto-sampler. Androgen was ionized using electrospray ionization in positive ion mode (ESI). The temperature of the drying gas in the ionization source was 225°C. The gas flow was 12 L/min, the nebulizer pressure was 35 psi, and the capillary voltage was 4000 V (positive) and 3000 V (negative). The analytes were quantified using multiple reaction monitoring with the mass transitions and parameters for each compound. Methanol and water were of LC-MS grade and all reagents were obtained from Thermo Fisher Scientific.

HPLC

High-performance liquid chromatography (HPLC) was performed as previously described (36). Briefly, cells were seeded and incubated in 24-well plate for ~24 h and then treated with the indicated drugs and [^{3}H]-labeled steroids (~1,000,000 cpm/well; PerkinElmer, Waltham, MA) at 37 °C. Aliquots of medium were collected and treated with β-glucuronidase (Novoprotein Scientific Inc, China) at 37 °C for 2h, extracted with ethyl acetate: isooctane (1:1), and dried in a freeze dryer (Martin Christ Gefriertrocknungsanlagen, Germany). Dried samples were reconstituted in 100 μL of 50% methanol and injected into the HPLC. Metabolites were separated on CORTECS C18 reverse-phase column (Waters, Ireland), using a methanol/water gradient at 40 °C. The column effluent was analyzed using β-RAM model 3 in-line radioactivity detector (LABLOGIC, USA). Results showed the mean and standard deviation (sd) value from one representative experiment. All HPLC studies were run in duplicate and repeated at least three times in independent experiments.

Gene expression assay

Cells were starved for at least 48 h with phenol red-free and 10% Charcoal stripped serum (Lonsera, China) and treated with DHEA, DHT, or pregnenolone (Steraloids Inc., US) or other drugs. Cell to cDNA Kit (EZBioscience, China) was used for cDNA synthesis directly from cells. Quantitative PCR (qPCR) experiment was conducted in Bio-Rad CFX96 (Bio-Rad), using EZBioscience 2× SYBR Green qPCR master mix (EZBioscience, China). The primers for qPCR have been showed in Table S5 and have been described in a previous study.[60] Results were presented as the mean and sd value from one representative experiment. All gene expression assays were performed in technical duplication and repeated at least three times in independent experiments.

AR competition assay

200,000 cells were seeded in 24-well plate and starved with phenol red-free medium and 5% CSS for 48 h. Cells were treated with 1nM [3H] R1881 and other steroids at indicated concentrations for 30 min. Intracellular radioactivity was measured with Tri-Carb® 5110TR Low Activity Liquid Scintillation Analyzer (PerkinElmer, Waltham, MA, USA) and protein concentration was detected by a microplate reader (BioTeK, Winooski, VT, US) at 562nm absorbance.

RNA-seq

Total RNA of each sample was extracted by TRIzol reagent (Invitrogen, Waltham, MA). VAHTSTM mRNA-seq V3 Library Prep Kit for Illumina (NR611) was used for library construction, following the manufacturer's instructions. In brief, 1000 ng of total RNA was used for purification and fragmentation of mRNA. Purified mRNA underwent first and second strand cDNA synthesis. cDNA was ligated to sequencing adapters (VAHTSTM RNA Adapters set3 - set6 for Illumina, N809/N810/N811/N812), and amplified by PCR (using 12 cycles). Final libraries were evaluated by Qubit Fluorometer (Invitrogen, Waltham, MA) and BioAnalyzer (Agilent 2100). Next, the sequencing was performed on HiSeq (PE150). The quality control of raw sequence data was evaluated by FastQC (v. 0.11.7), and quality trimming and adapter clipping by Trimmomatic (v.0.36-5). Paired-end reads were aligned to the GRCh38.91 human reference genome using hisat2 (v.2-2.1.0). The gene expression level was quantified by HTSeq (v.0.11.1). Normalization of counts was done using the DESeq2 (v.1.24.0). Differential expression analyses were performed using DESeq2 based on the gene read count data. Biology duplication were used for each treatment.

GSEA analysis and ChIP-seq analysis

The normalized counts were prepared for gene set enrichment analysis (GSEA). Gene set of "VCaP_DHT_UP.grp" was derived from top 1000 upregulated genes (log2FoldChange > 1; FDR < 0.05) when induced by DHT in VCaP.

Genes were ranked by "Ratio_of_Classes," and the permutation type was "gene set" and other sets using the GSEA default. The thresholds for inclusion were $p < 0.05$ and $q < 0.25$. GSEA was performed using the JAVA program (http://software.broadinstitute.org/gsea/downloads.jsp) and run in pre-ranked mode to identify enriched signatures. The GSEA plot, normalized enrichment score and FDR and q values were derived from GSEA output.

ChIP-Seq genomic traces were generated using IGV for visualization. Data (normalized bigwig files) were downloaded from the public database Cistrome, and the biological duplicate samples were combined and averaged.

Cell proliferation assay

Cells were starved for at least 48 h with phenol red-free and 10% Charcoal stripped serum (Lonsera, China) and then treated with indicated drugs. Cell proliferation assay was performed with cell counting kit-8 (Beyotime, China), in accordance with the manufacturer's instructions. Briefly, 20,000 cells/well dispensed in 100 μL aliquots were seeded in a 96-well plate. The viable cell count was measured according to the manufacturer's protocol. The absorbance was read at 450 and 600 nm, using a microplate reader (BioTeK, US). The growth curve was calculated by Graphpad Prism 8.0 software (San Diego, CA, US). Results were represented as the mean and SD value from one representative experiment. Experiments were performed in five replication and repeated at least three times independently.

Pyrosequencing

DNA was extracted with QIAamp DNA Mini Kit (QIAGEN) and pyrosequencing was performed by Genergy Biotechnology (Shanghai, China). Briefly, genomic DNA of VCaP was treated with bisulfite conversion using Qiagen EpiTect® Bisulfite Kit (QIAGEN). Primers selectively amplified either methylated or unmethylated DNA were used. PCR products were sequenced on PyroMark Q96 ID (QIAGEN).

QUANTIFICATION AND STATISTICAL ANALYSIS

The percentage of each metabolite was calculated as follows: metabolite/ (abiraterone + abiraterone metabolites) × 100% in Figures 2, 3, and 6. Statistical analyses between groups were performed using the Student's t-test. Gehan-Breslow-Wilcoxon test was used to calculate the p value for PSA biochemical recurrence. *, $p < 0.05$; **, $p < 0.01$. All analyses were performed using GraphPad Prism® 8.0 software. Data represent mean ± SD, unless indicated specifically. There were no method were used to determine whether the data met assumptions of the statistical approach.